Jack mackerel acoustic density index in the central-north acoustic surveys, estimated using spatiotemporal models with sdmTMB.

By Ignacio Payá y Víctor Catasti

May 2026.

Stock Assessment Department.

Chilean Fisheries Development Institute.

Abstract

The series of hydroacoustic survey cruises for jack mackerel in the northern zone is one of the main indices used to inform the stock assessment model (JJM). This series has changed over time with respect to the spatial extent of the study areas, the number of basic sampling units, and the incorporation of sporadic transects to intensify the sampling grid in areas of higher jack mackerel density, as well as to explore new areas.

The objective of this study was to estimate the historical time series of acoustic density of jack mackerel in the northern zone using spatiotemporal models implemented through the sdmTMB framework. Five models were fitted; the best-performing model (model 5) included a fixed year effect and a smoother for oxygen concentration (s(Oxg)), combined with spatiotemporal first-order autoregressive covariance (AR1) and anisotropy.

The trend of the acoustic density index (Sa) estimated from Model 5 was consistent with the trend of density (t/nm²) estimated annually using the biomass estimation method. This is a notable result, as these series are not fully comparable: acoustic density represents the raw acoustic signal, whereas density expressed in tonnes results from the integration of the acoustic signal with biological information. Consequently, observed differences between both indices may be attributed to changes in population size structure and variations in the condition factor of the fish.

A similarity was also observed between the trend of the acoustic density index (Sa) and the trend of total biomass estimated annually using the hydroacoustic biomass estimation method. In this case, in addition to the effects of biological information and the target strength relationship, the effect of the area used in the estimation of total biomass must also be considered.

Under these conditions, the acoustic density index may be particularly informative when the number of trawl hauls is low and when spatiotemporal sampling of length distributions may be biased.

Contents

1. Background

The series of hydroacoustic survey cruises for jack mackerel in the northern zone is one of the main indices used to inform the stock assessment model (JJM) about trends in abundance by age group. This series has changed over the years in the spatial extent of the study areas, the number of basic sampling units (BSU), and the incorporation of new sporadic transects to intensify the grid in areas of higher jack mackerel density, as well as to explore new areas. All these grid changes may affect the spatiotemporal estimates of jack mackerel density.

The sdmTMB package allows the implementation of spatial geostatistics and spatio-temporal generalized linear mixed models (Anderson et al. 2022), using TMB to fit the model and INLA to construct the SPDE (stochastic partial differential equation).

2. Objective

To estimate the historical series of acoustic density of jack mackerel in the northern zone using spatiotemporal models implemented with the sdmTMB framework.

3. Methods

3.1. Database

The database was provided by Víctor Catasti, Chief Scientist of Acoustic Surveys, and included acoustic records per basic sampling unit (BSU) and environmental variables (temperature, salinity, and oxygen) from 2010 to 2024. The number of transects and BSUs has changed substantially over the time series. Transects 1 to 33 are the most stable and have the largest number of records (Table 1). Transects 51 to 83 correspond to coastal navigation transects (Table 2); transects 101 to 133 correspond to oceanic navigation; and transects greater than 400 are those applied to intensify the sampling grid where high jack mackerel densities were observed.

Table 1. Number of records per year for the most stable transects.

Count of Longitud	Column Labels														
Row Labels	2010	2011	2012	2013	2014	2015	2016	2017	2018	2019	2020	2021	2023	2024	Grand Total
1	198	139	200	202	168	201	219	191	198	181	213	249	401	217	2977
2	133	177	196	198	210	178	201	197	198	215	198	212	392	261	2966
3	199	179	200	200	219	197	197	194	194	177	196	244	429	217	3042
4	201	180	198	197	199	177	196	305	196	179	194	221	377	207	3027
5	189	180	199	198	230	198	199	104	194	180	194	237	384	213	2899
6	199	180	199	199	206	198	196	197	194	169	196	186	489	219	3027
7	173	178	198	201	203	198	198	200	194	185	201	306	386	204	3025
8	168	194	200	197	222	197	198	219	223	170	214	414	389	241	3246
9	201	174	198	198	204	199	245	198	199	182	204	247	357	210	3016
10	207	193	205	198	204	198	243	212	233	181	202	262	434	211	3183
11	209	178	199	198	76	198	198	222	200	180	199	218	399	219	2893
12	199	191	198	198	147	201	244	228	215	180	201	260	393	204	3059
13	201	192	200	198	152	197	198	232	200	212	188	231	361	220	2982
14	200	198	197	198	454	197	228	241	229	230	190	268	413	257	3500
15	189	198	198	198	204	198	198	235	199	229	217	234	459	205	3161
16	186	198	198	198	184	199	197	199	238	223	280	235	434	254	3223
17	195	195	198	199	228	200	204	203	253	180	255	231	374	203	3118
18	197	198	201	198	206	198	201	198	200	179	249	225	396	218	3064
19	201	202	198	199	214	192	199	199	199	180	214	220	385	245	3047
20	199	200	196	198	199	188	199	198	240	179	200	264	364	234	3058
21	202	200	198	199	199	188	207	197	235	178	206	217	408	216	3050
22	206	214	186	198	202	188	204	198	230	178	213	209	375	246	3047
23			197	198	230	188	82	209	200	210	214	201	246	214	2389
24			196	198	204	158	187	198	178	204	204	138	302		2167
25					214		198	198	200	199	198		453	198	1858
26					379		178	201	188	198	199		375	206	1924
27							177	178	199	198	178		283	195	1408
28							179	178	198	198	180		272	231	1436
29							178	180	199	203	203		313	227	1503
30							184	181	198	198	198		234	238	1431
31							177	178	229	198	201		272	214	1469
32							198	184	157	199	191		294	242	1465
33							158	158	136	154	126		221	150	1103
Grand Total	**4252**	**4138**	**4753**	**4763**	**5557**	**4631**	**6465**	**6610**	**6743**	**6306**	**6716**	**5729**	**12064**	**7036**	**85763**

Table 2. Number of records per year for coastal navigation transects.

Count of Longitud	Column Labels													
Row Labels	2010	2011	2012	2013	2014	2015	2016	2017	2018	2019	2020	2021	2023	2024	Grand Total
51	47						68								115
52	55	48	54	49	104	63	54	59	52	52	51	53	90	55	839
53									101						101
54	55	63	50	51	53	54	58	54	54	52	51	55	51	85	786
55									50						50
56	55	49	56	56	76	52	54			52	61	55	54	101	721
57						25		74	66					80	245
58	50	50	58	59		55	72			52	57	57	111	71	692
59					49			60	74						183
60		54	71	58		58	55			56	52	72	88	61	625
61	63	66			22			64	65						280
62	56		49	51		54	54			54	57	71	92	108	646
63		50						63	60						173
64	51		54	51		65	50			51	52	61	83	75	593
65		65						59	60						184
66	55		52	51		62	76			53	55	56	78	123	661
67		53			12			61	53						179
68	40		68	53		70	60			59	57	59	55	57	578
69		52			3			58	58						171
70			111	62	10	131	53			52	35	50	91	99	694
71	113	52			2			50	50						267
72			101	106		110	50			51	54	54	77	54	657
73					3		58	68	53	34	23				239
74						122		80		80	75		86		443
75					16		52		51						119
76								59		51	51		78	72	311
77							51		51						102
78								61		52	57		89	65	324
79							53		52						105
80								106		104	102		129	126	567
81							111		103		60				274
82										101	101		140	117	459
83									104		202				306
Grand Total	**640**	**602**	**724**	**647**	**350**	**921**	**1029**	**976**	**1157**	**1006**	**1253**	**643**	**1392**	**1349**	**12689**

Table 3. Number of records per year for oceanic navigation transects.

Count of Longitud	Column Labels														
Row Labels	2010	2011	2012	2013	2014	2015	2016	2017	2018	2019	2020	2021	2023	2024	Grand Total
101									50	49	50	51	103	51	354
103									49	51	50	50	50	50	300
105									49	49		52	51	50	251
106									74						74
107										68	59	59	61	59	306
108									58						58
109										54		58	54	55	221
110									50						50
111										58		84	54	62	258
112									54						54
113										51	56	52	90	50	299
114									55						55
115										62	54	56	56	54	282
116									49						49
117										49	52	49	51	52	253
118									50						50
119										51		51	52	52	206
120									56						56
121										50	54	60	50	55	269
122									61						61
123										50	53	70	57		230
124									51						51
125										50	50		63	51	214
126									49						49
127										50			58	51	159
128									50						50
129										49	50		51	50	200
130									72						72
131										100			136	101	337
132									100						100
133														123	123
Grand Total									**977**	**891**	**528**	**692**	**1037**	**966**	**5091**

Table 4. Number of records per year for transects used to intensify the grid where high jack mackerel densities were observed.

Count of Longitud	Column Labels														
Row Labels	2010	2011	2012	2013	2014	2015	2016	2017	2018	2019	2020	2021	2023	2024	Grand Total
411														10	10
417														11	11
501												4	208	21	233
502													128		128
503												12	101		113
504												3			3
505												3			3
506												3			3
507												7			7
508												6			6
511												7			7
512												2			2
513												2			2
514												8			8
601												52			52
602												158			158
603												71			71
604												90			90
605												60			60
801												33			33
804												15			15
805												18			18
806												9			9
810														9	9
812														6	6
816														35	35
818														23	23
902														51	51
903												78			78
904												179		73	252
905												172			172
Grand Total												**992**	**437**	**239**	**1668**

To apply the same criteria used in IFOP estimation procedures, as communicated personally by Víctor Catasti, the database was restricted up to transect no. 121 to exclude some sporadic transects extending westward at the northern boundary of the study area. In this way, the usual transects, coastal navigation transects, and oceanic navigation transects were included. In addition, records with missing values (NaN) for environmental variables were excluded; specifically, records with temperatures below 12°C were removed. The resulting dataset was named "cjmST".

Latitude and longitude positions were transformed to UTM (Mercator projection) using EPSG: 32718 – WGS 84 / UTM zone 18S (https://maps.omniscale.com/en/openstreetmap/epsg-32718) (Figure 1).

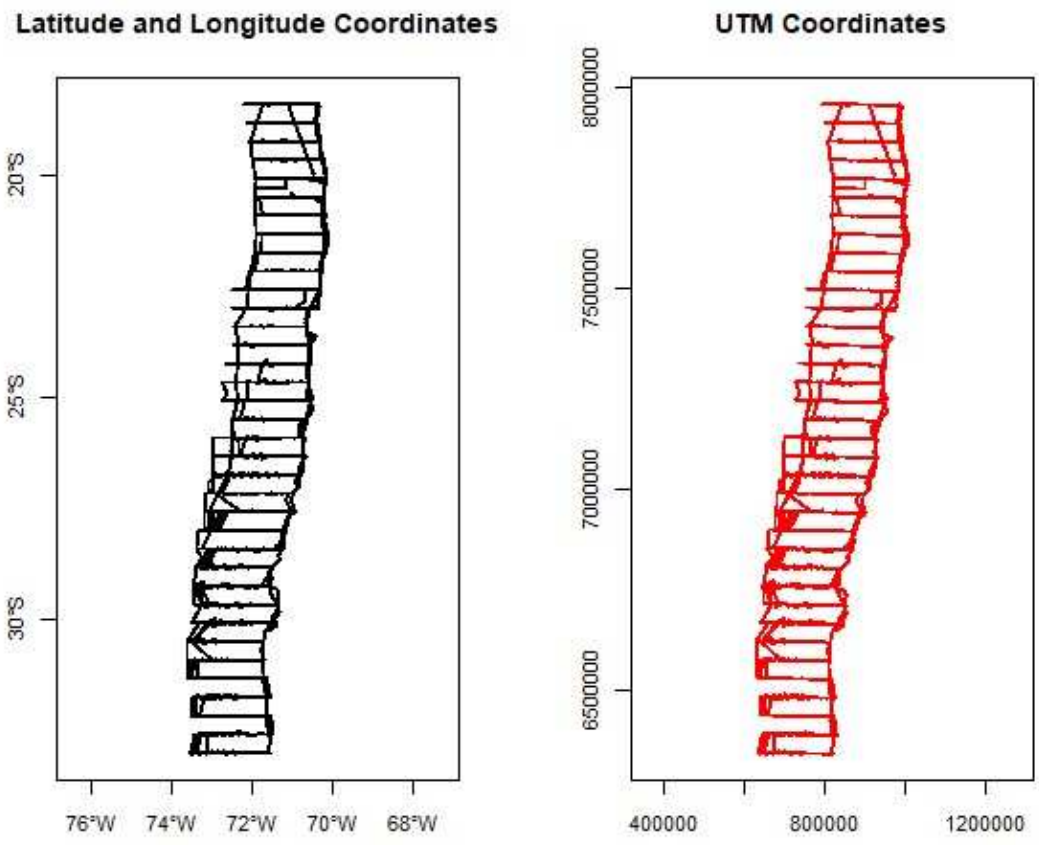

Figure 1. Location of BSUs in latitude/longitude and in UTM.

3.2. Estimation meshes

To discretize space, a mesh was constructed to generate a set of neighboring points at which spatial autocorrelation can be evaluated. A triangular mesh was used because it is more flexible and can adapt to irregular domains.

The SPDE (Stochastic Partial Differential Equation) approach was used to represent the spatial autocorrelation structure of the database at the mesh vertices. In this framework, the SPDE provides a computationally efficient representation of a Matérn Gaussian random field. The Matérn covariance function can be written as:

$$Cov(S(x_i), S(x_j)) = \frac{\sigma^2}{2^{\upsilon-1}\Gamma(\nu)} (\kappa \|x_i - x_j\|)^{\nu} \kappa_{\nu}(\kappa \|x_i - x_j\|)$$

where K_ν(·) is the modified Bessel function of the second kind of order ν>0; ν is the smoothness parameter; σ^2 is the marginal variance; and κ>0 is a spatial scale parameter related to the practical range. The practical range is commonly defined as ρ = √(8ν)/κ, i.e., the distance at which the spatial correlation is approximately 0.1.

Estimation meshes affect precision and computational time; therefore, different meshes were evaluated. The mesh automatically generated by sdmTMB was too dense (Figure 2), so the number of intersections was reduced (Figure 3), and finally a boundary polygon was added to restrict estimates to the study area (Figure 4).

The mesh specification used was:

```
mesh_6 <- make_mesh(   cjmST, c("X", "Y"),  fmesher_func = fmesher::fm_mesh_2d_inla,
                boundary = bnd,   cutoff = 25,  max.edge = c(200, 400),  offset = c(5, 40) )
```

where boundaries (bnd) were estimated as:

```
bnd <- INLA::inla.nonconvex.hull(cbind(cjm$X, cjm$Y), convex = -0.5/30)
```

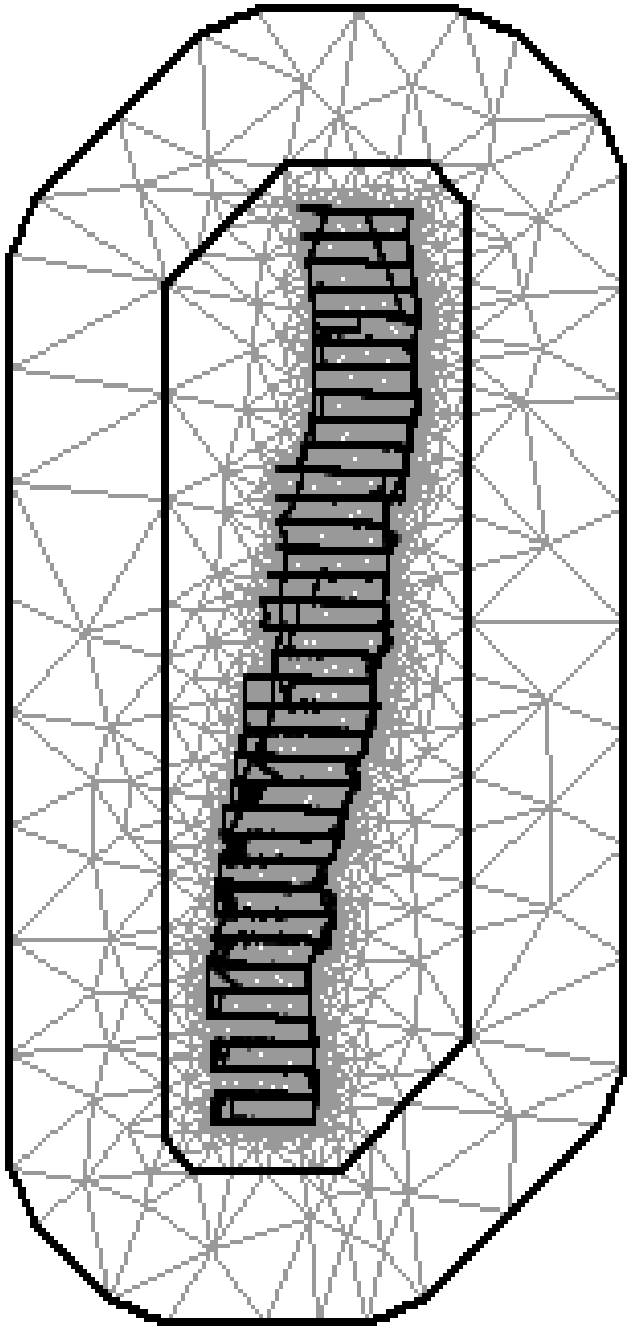

Figure 2. Default mesh generated automatically by sdmTMB.

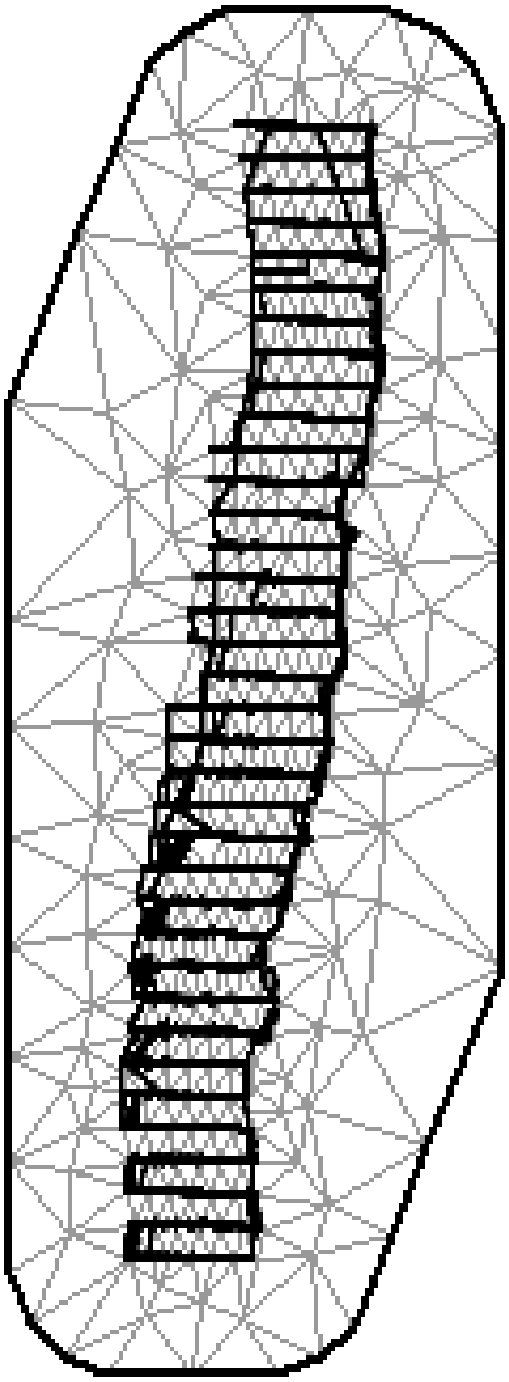

Figure 3. Mesh generated with a smaller number of intersections.

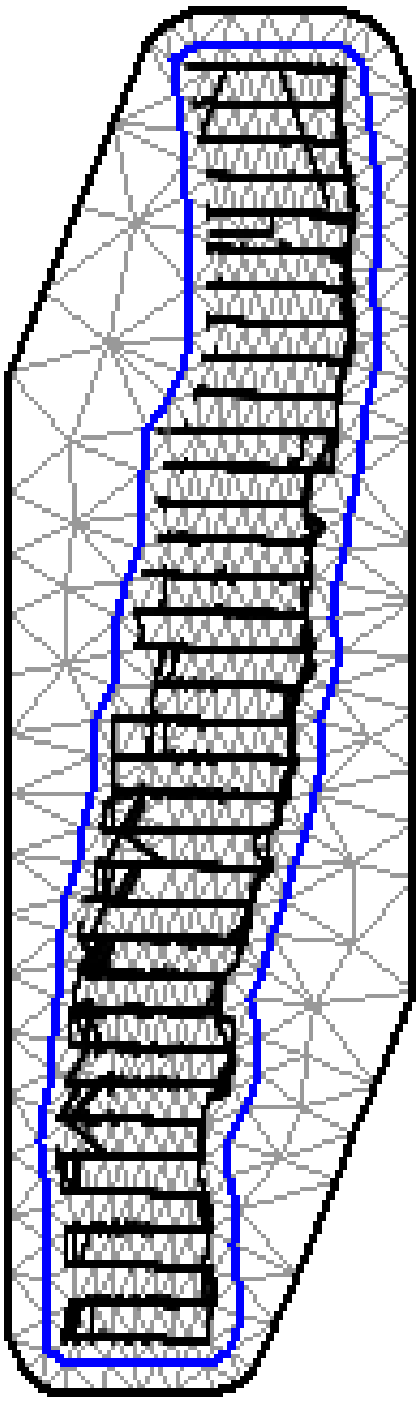

Figure 4. Mesh used with estimates restricted to the interior of the blue polygon.

Acoustic density (JM_Sa) distributions were log-normal with a high proportion of zeros and annual maximum values that increased in more recent years (Figure 5). Therefore, a Tweedie distribution was used (McCullagh & Nelder, 1989; Dunn, 2017).

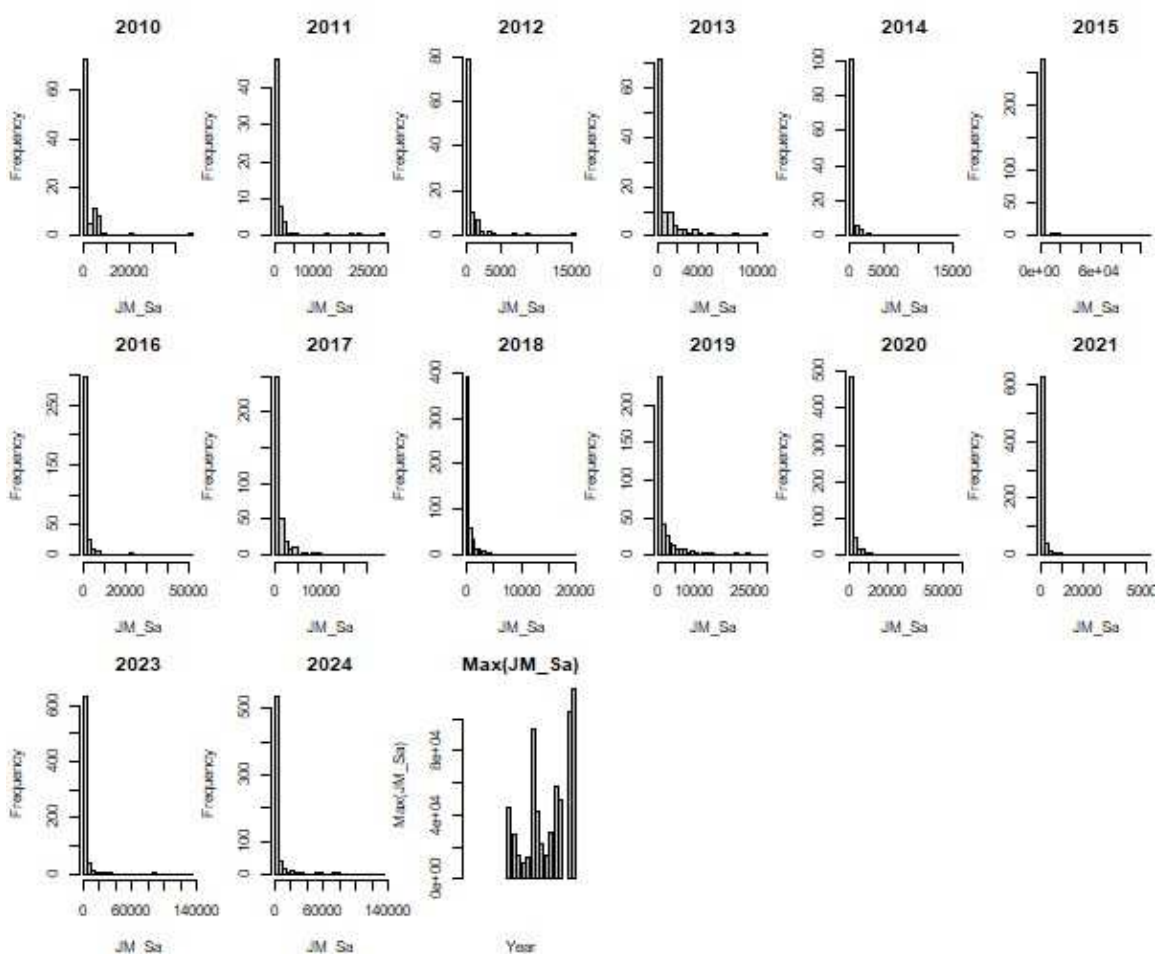

Figure 5. Histograms of acoustic density (JM_Sa) by year, and annual maximum values (Max(JM_Sa)) (last panel).

3.3. Statistical models.

Model 1. Surface sea temperature (SST) effect with spatial covariance and isotropic.

The model 1 was:

$$E\left[y_{s,t}\right] = \mu_{s,t},$$

$$g(\mu_{s,t}) = s(SST) + \omega_s,$$
$$\omega_s \sim MVNormal(0, \Sigma_\omega),$$

where the link function of the acoustic density $g(\mu_{s,t})$ is the related with the spline of SST ($s(SST)$), and ω_s are iid spatial random fields.

Model 1 in sdmTMB syntax was:

```
fit1 <- sdmTMB( JM_Sa ~ s(SST), data = cjmSST, family = tweedie(link = "log"), mesh = mesh,
      spatial = "on")
```

where JM_Sa is acoustic density, and s(SST) is a smoother ("spline") for temperature (SST). Spatial position is modeled as a random effect. The link function is "log" for a Tweedie error distribution (continuous density with zeros).

Model 2. Salinity (Sal) effect with spatial covariance and anisotropic.

Similar to model 1 but with salinity and anisotropy.

```
fit2 <- sdmTMB( JM_Sa ~ s(Sal), data = cjmST, family = tweedie(link = "log"), mesh = mesh,
spatial = "on", anisotropy = TRUE)
```

Model 3. Oxygen concentration (Oxg) effect with spatial covariance and anisotropy.

Similar to model 2 but with Oxygen.

```
fit3 <- sdmTMB( JM_Sa ~ s(Oxg),  data = cjmST,  family = tweedie(link = "log"),  mesh =
mesh,  spatial = "on",  anisotropy = TRUE)
```

Model 4. Oxygen concentration (Oxg) effect with spatio-temporal first-order autoregressive covariance (AR1) and anisotropy.

Model 4 was:

$$g(\mu_{s,t}) = S(Oxg, k = 5) + \delta_{s,t},$$
$$\delta_{t=1} \sim MVNormal(0, \Sigma_\epsilon),$$
$$\delta_{t>1} \sim \rho\delta_{t-1} + \sqrt{1-\rho^2}\epsilon_t, \ \epsilon \sim MVNormal(0, \Sigma_\epsilon)$$

where g(·) is the link function; μ is the mean acoustic density (Sa); s denotes spatial location (x and y coordinates); t is time; S(·) is a smoothing spline with basis dimension k; δ are spatiotemporal deviations; Σ_ϵ is the covariance matrix of the spatiotemporal random fields; and ρ is the correlation between consecutive spatiotemporal fields. This scaling yields a steady-state (marginal) variance. The parameter ρ allows mean-reverting spatiotemporal fields and is constrained to $-1 < \rho < 1$.

```
fit4 <- sdmTMB(  JM_Sa ~ s(Oxg), data = cjmST, mesh = mesh, time = "Year", family =
      tweedie(link = "log"), spatial = "off", spatiotemporal = "ar1", extra_time = c(2022),
      anisotropy = TRUE )
```

Model 5. Fixed year effect and oxygen concentration (Oxg), with spatio-temporal first-order autoregressive covariance (AR1) and anisotropy.

Moel 5 was:

$$g(\mu_{s,t}) = \mathrm{X}_{s,t}^{\mathrm{main}}\beta + S(Oxg, k=5) + \delta_{s,t},$$
$$\delta_{t=1} \sim MVNormal(0, \Sigma_\epsilon),$$
$$\delta_{t>1} \sim \rho\delta_{t-1} + \sqrt{1-\rho^2}\epsilon_t, \ \epsilon \sim MVNormal(0, \Sigma_\epsilon)$$

where $\mathrm{X}_{s,t}^{\mathrm{main}}$ is the design matrix for the main effect (year), β is the fixed-effect coefficient vector.

```
fit5 <- sdmTMB( data = cjmST, formula = JM_Sa ~ 0 + as.factor(Year) + s(Oxg),  time = "Year",
      mesh = mesh_6,  family = tweedie(link = "log"),  spatiotemporal = "ar1",  extra_time =
      c(2022),  anisotropy = TRUE)
```

extra_time is used to define the year without data that should estimate by the model.

Based on Model 5, the index was estimated using the prediction function applied to the original data and an area of 2 × 2 kilometers. This index corresponds to the sum of the acoustically predicted values over the entire grid. This was specified in sdmTMB as follows:

```
index <- get_index(predictions, area = 4, bias_correct = TRUE)
```

The Sa index was also estimated for the northern area (≤25.92°S).

4. Results

The best model according to the AIC criterion was Model 5 (Table 5). Estimated parameters are presented in Table 6, and the model fit quality (sanity check) is shown in Table 7.

Table 5. Model comparison using Akaike (AIC).

Modelo	Código	df	AIC
Modelo 1	fit1	7	117209.2
Modelo 2	fit2	9	117195.1
Modelo 3	fit3	9	116995.2
Modelo 4	fit4	10	109135.0
Modelo 5	**fit5**	**24**	**109107.6**

Table 6. Summary of Model 5 specification and estimated parameters.

Spatiotemporal model fit by ML ['sdmTMB']
Formula: JM_Sa ~ 0 + as.factor(Year) + s(Oxg)
Mesh: mesh_6 (anisotropic covariance)
Time column: Year
Data: cjmST
Family: tweedie(link = 'log')

	coef.est	coef.se
as.factor(Year)2010	-10.31	1.98
as.factor(Year)2011	-9.92	2.53
as.factor(Year)2012	-7.70	1.73
as.factor(Year)2013	-10.65	1.88
as.factor(Year)2014	-10.82	1.80
as.factor(Year)2015	-6.47	1.68
as.factor(Year)2016	-5.89	1.50
as.factor(Year)2017	-6.88	1.50
as.factor(Year)2018	-4.51	1.42
as.factor(Year)2019	-5.55	1.49
as.factor(Year)2020	-4.53	1.40
as.factor(Year)2021	-2.26	1.60
as.factor(Year)2023	-3.56	1.44
as.factor(Year)2024	-3.98	1.44
sOxg	5.95	5.87

Smooth terms:

	Std. Dev.
sds(Oxg)	26.17

Dispersion parameter: 97.90
Tweedie p: 1.61
Spatiotemporal AR1 correlation (rho): 0.06
Matérn anisotropic range (spatial): 58.1 to 173.3 at 86 deg.

Spatial SD: 2.50
Spatiotemporal marginal AR1 SD: 6.95
ML criterion at convergence: 54529.781

Table 6. Model 5 fit diagnostics (sanity checks).

✓ Non-linear minimizer suggests successful convergence
✓ Hessian matrix is positive definite
✓ No extreme or very small eigenvalues detected
✓ No gradients with respect to fixed effects are >= 0.001
✓ No fixed-effect standard errors are NA
✓ No standard errors look unreasonably large
✓ No sigma parameters are < 0.01
✓ No sigma parameters are > 100
✓ Range parameter doesn't look unreasonably large

Table 7. Estimates of fixed effects (Years).

	term	estimate	std.error	conf.low	conf.high
1	as.factor(Year)2010	-10.3	1.98	-14.2	-6.43
2	as.factor(Year)2011	-9.92	2.53	-14.9	-4.95
3	as.factor(Year)2012	-7.70	1.73	-11.1	-4.31
4	as.factor(Year)2013	-10.7	1.88	-14.3	-6.96
5	as.factor(Year)2014	-10.8	1.80	-14.3	-7.30
6	as.factor(Year)2015	-6.47	1.68	-9.77	-3.18
7	as.factor(Year)2016	-5.89	1.50	-8.84	-2.95
8	as.factor(Year)2017	-6.88	1.50	-9.82	-3.93
9	as.factor(Year)2018	-4.51	1.42	-7.28	-1.74
10	as.factor(Year)2019	-5.55	1.49	-8.47	-2.64
11	as.factor(Year)2020	-4.53	1.40	-7.27	-1.79
12	as.factor(Year)2021	-2.26	1.60	-5.40	0.881
13	as.factor(Year)2023	-3.56	1.44	-6.39	-0.734
14	as.factor(Year)2024	-3.98	1.44	-6.80	-1.15

Table 7. Estimates of random effects and Matérn model parameters.

	term	estimate	std.error	conf.low	conf.high
1	range	100.	6.73	88.0	114.
2	phi	97.9	1.47	95.1	101.
3	sigma_O	2.50	0.311	1.95	3.19

4	sigma_E	6.95	0.298	6.39	7.56
5	tweedie_p	1.61	0.00333	1.61	1.62
6	rho	0.0621	NA	-0.0286	0.152

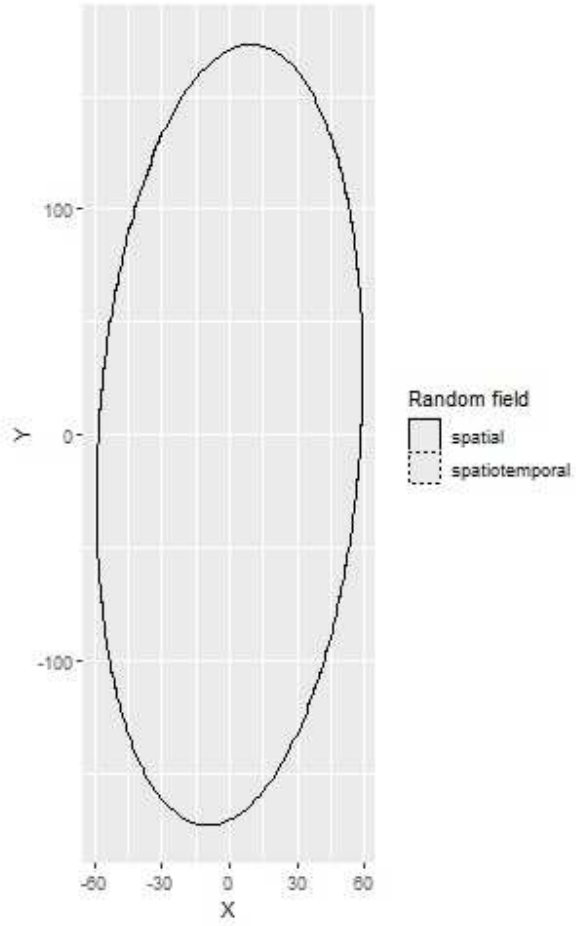

Figure 6. Anisotropic pattern.

Predictions (fixed effects plus spatiotemporal random effects) at BUS locations are shown in Figure 7.

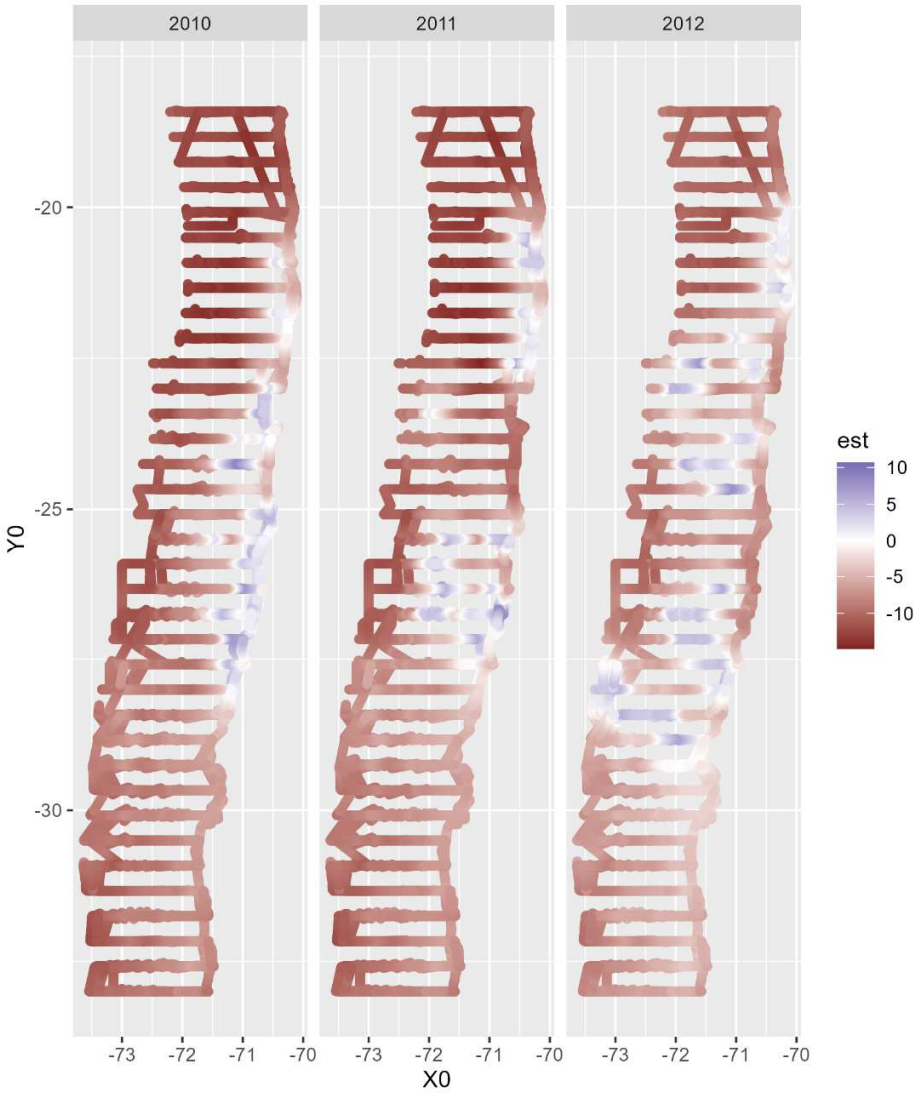

Figure 7. Predictions (fixed effects plus spatiotemporal random effects) in logarithmic scale by year (panels).

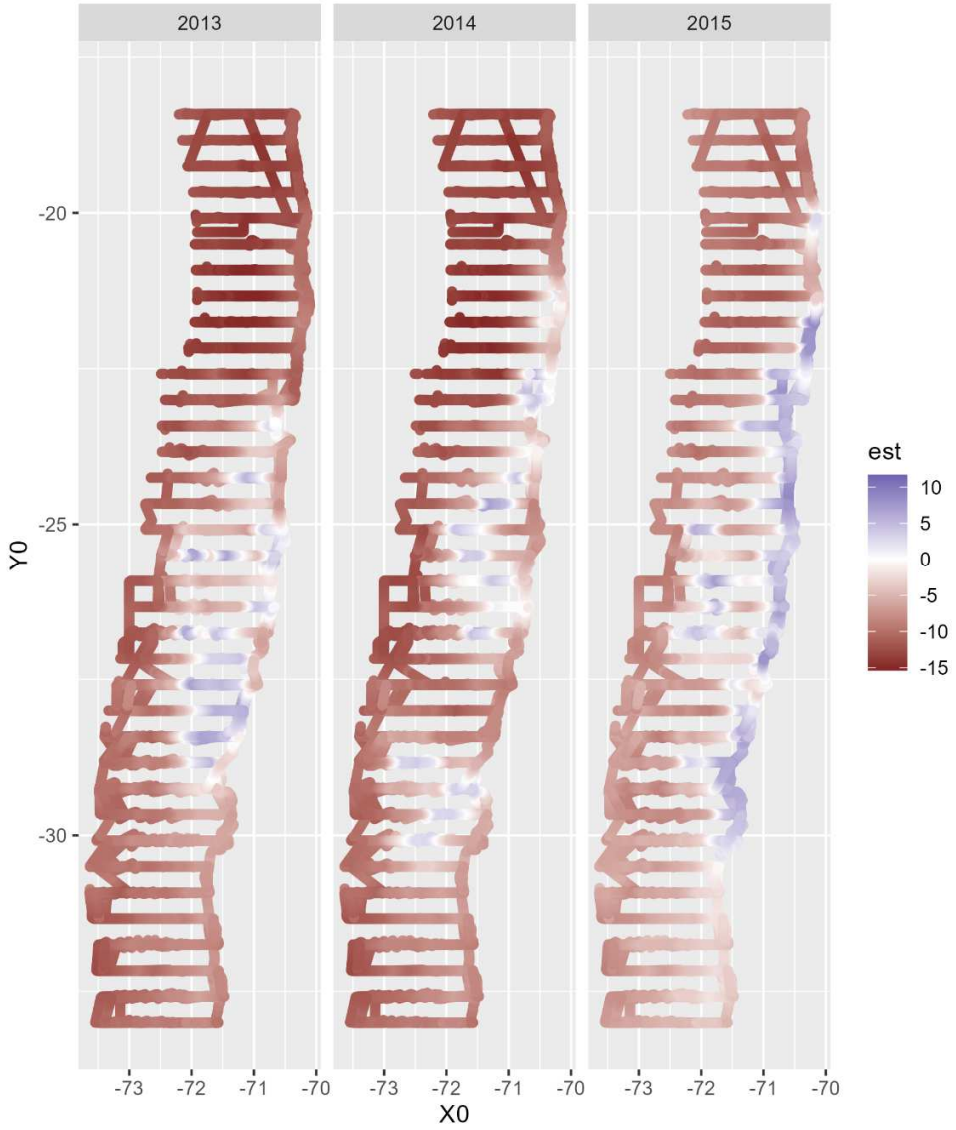

Figure 7. Continued

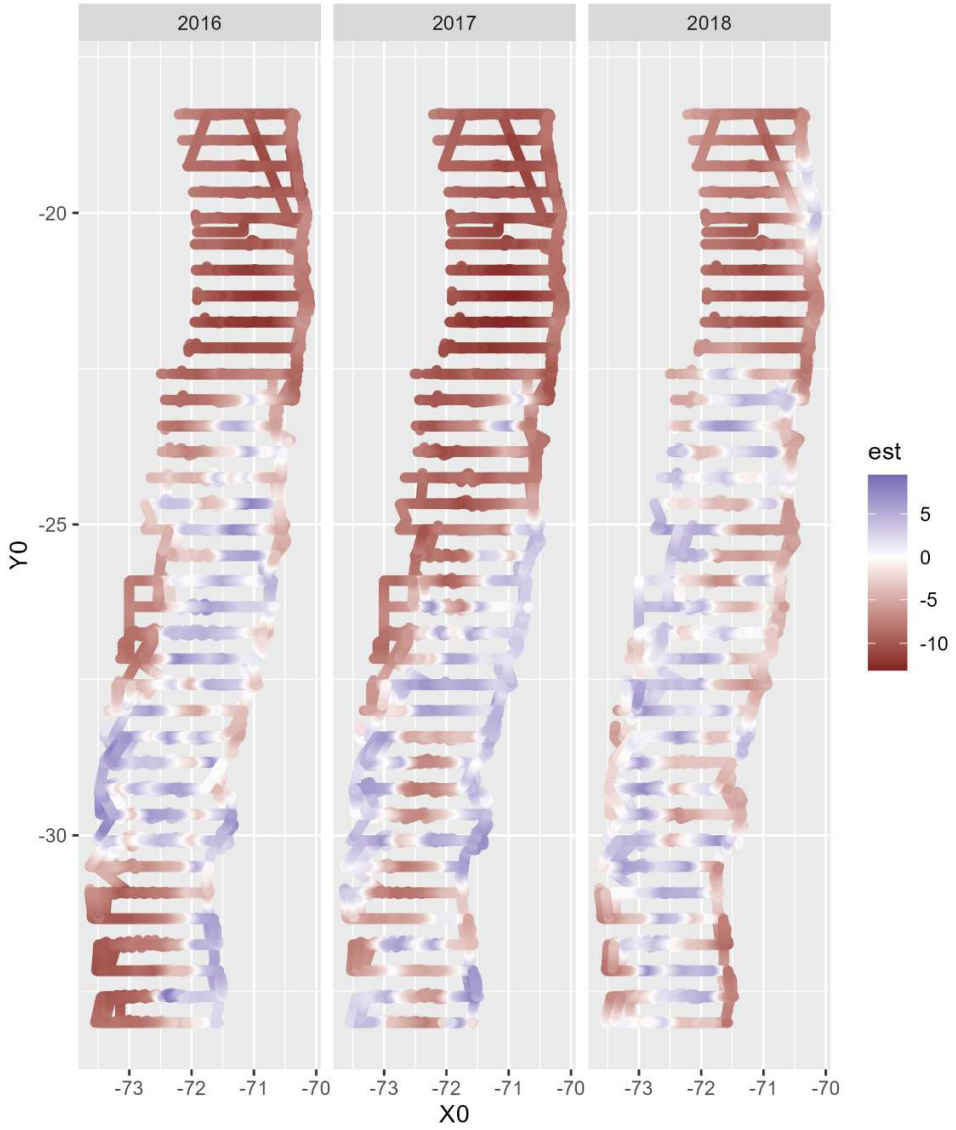

Figure 7. Continuated

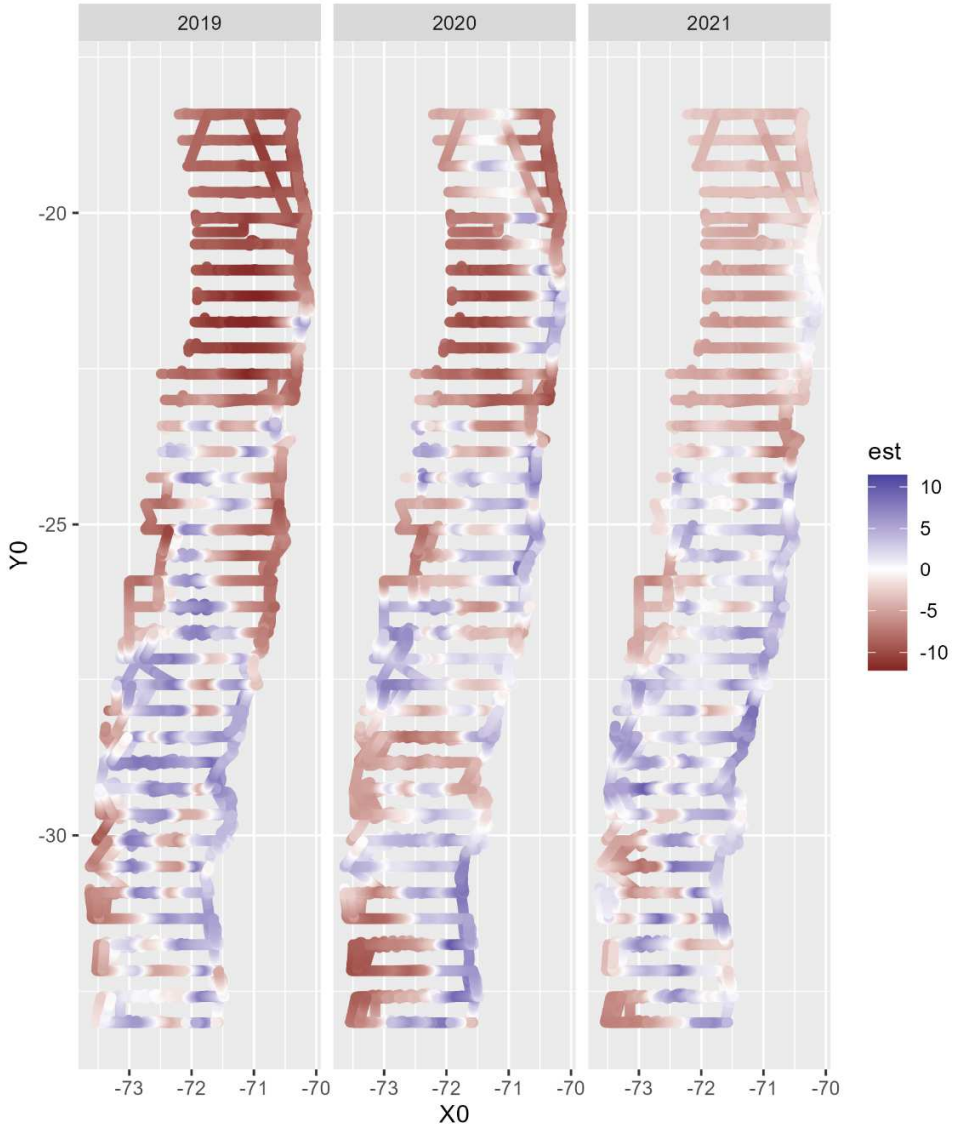

Figure 7. Continuated

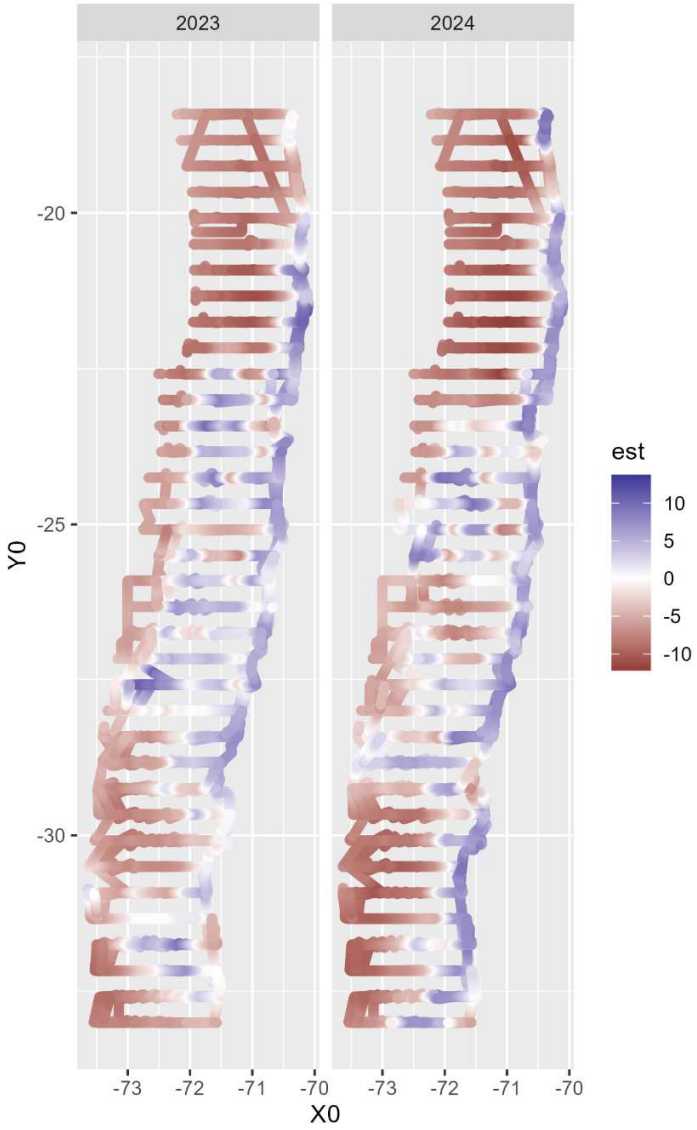

Figure 7. Continuated.

The model residuals are shown in Figure 8.

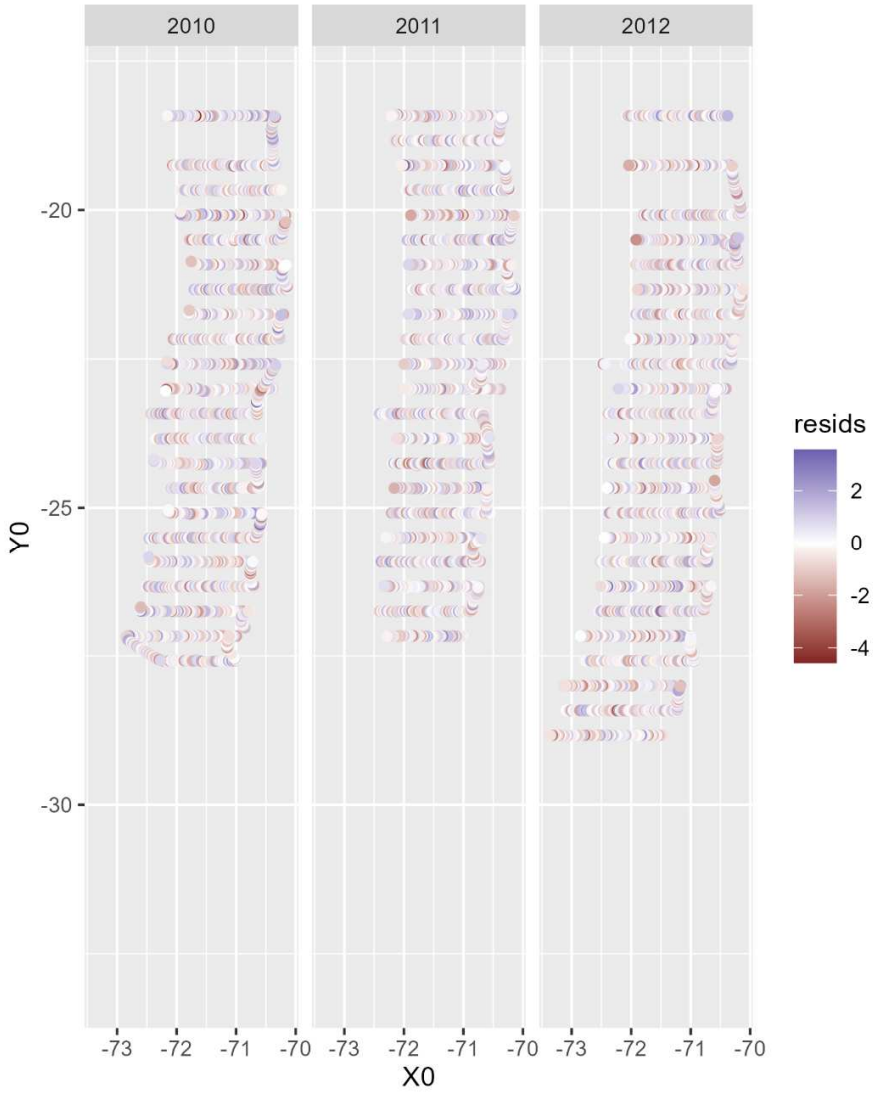

Figure 8. Residuals by year.

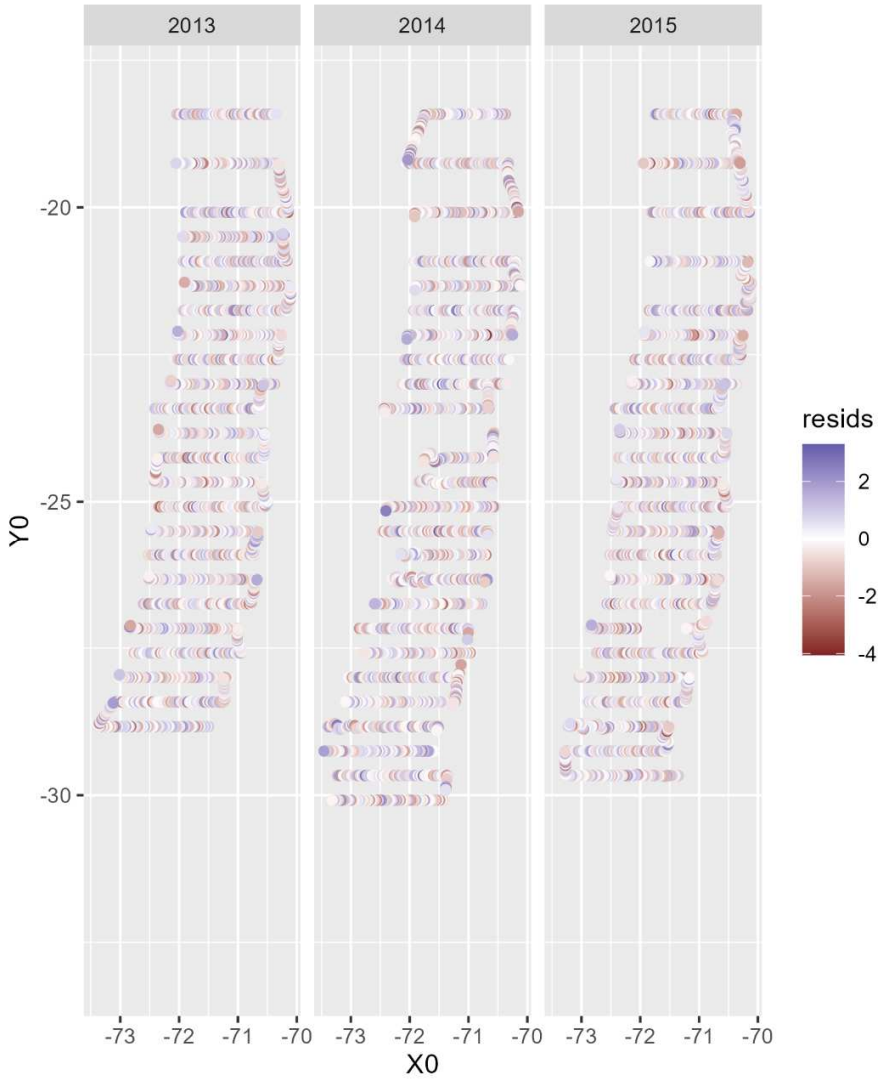

Figure 8. Continuated

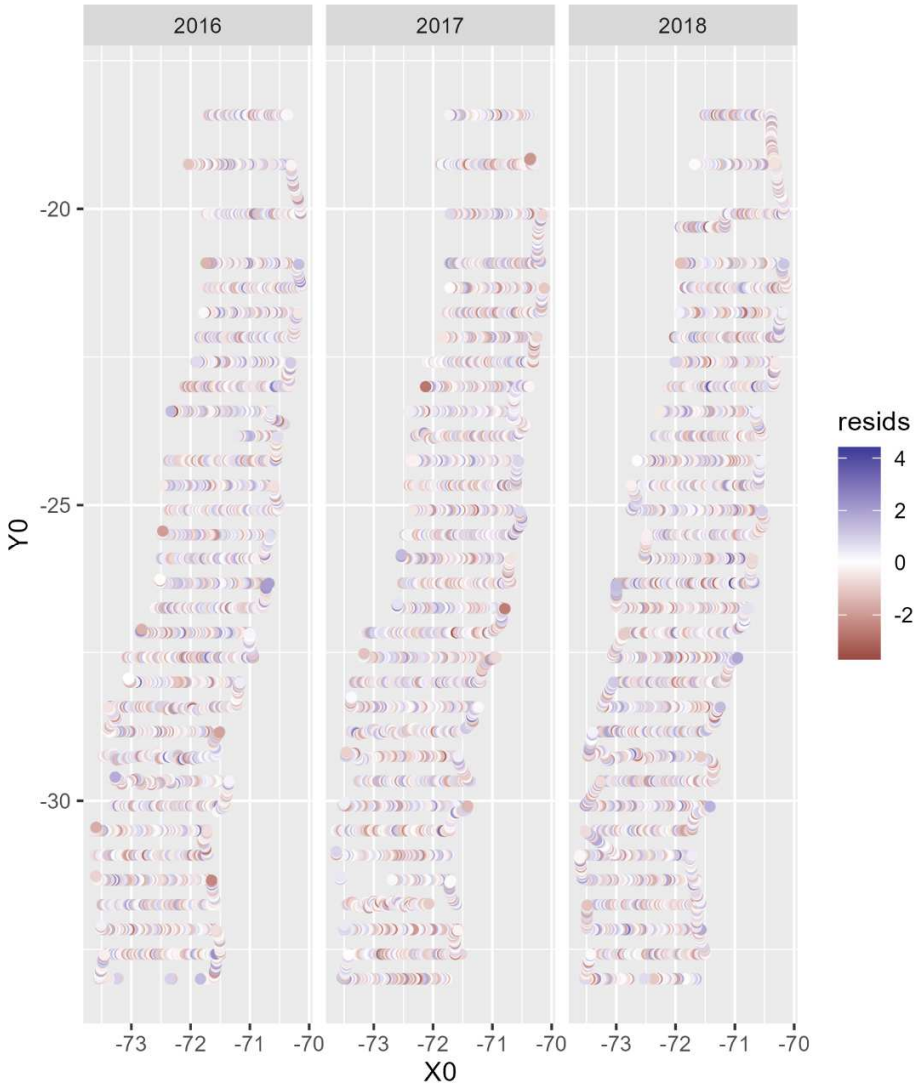

Figure 8. Continuated

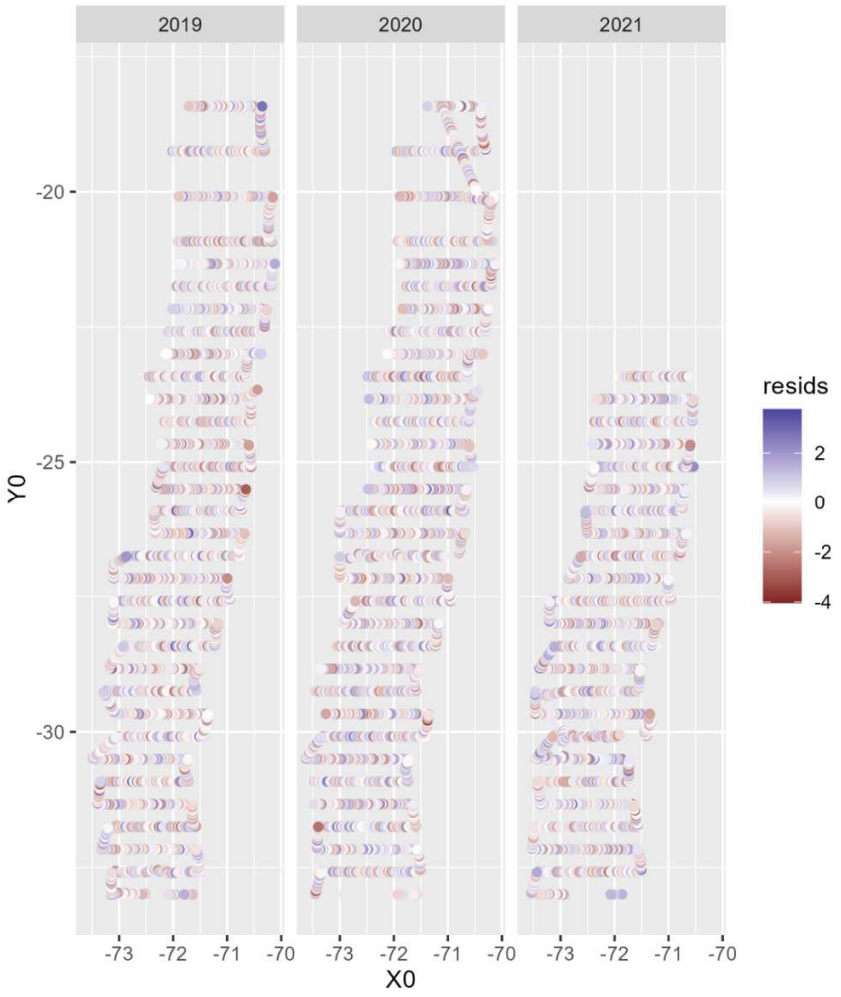

Figure 8. Continuated

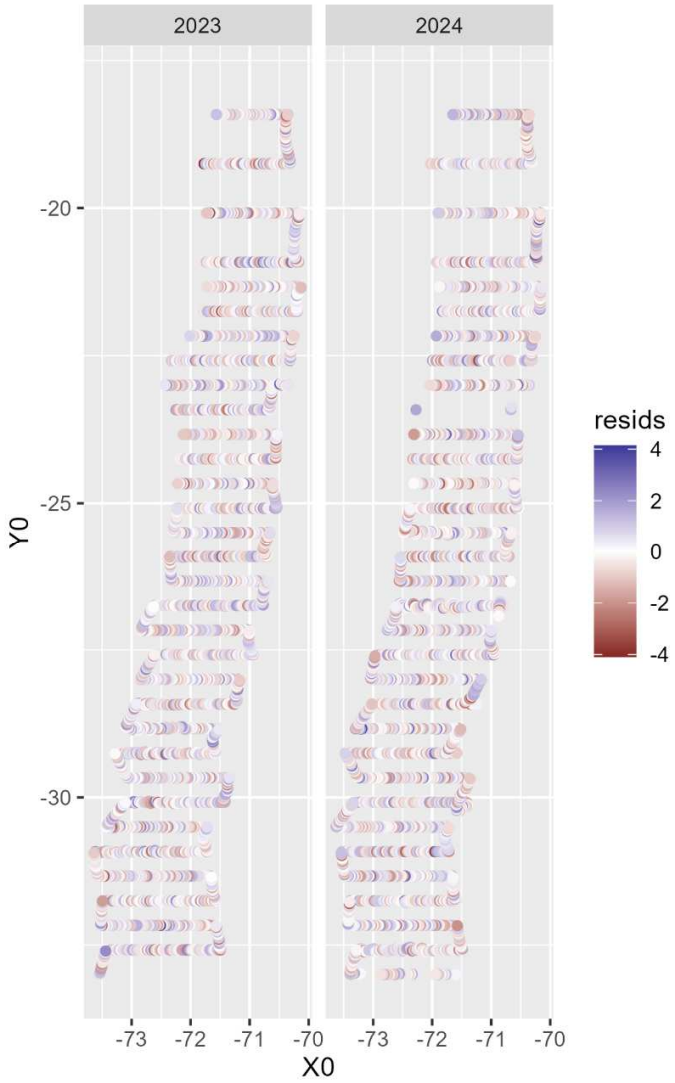

Figure 8. Continuated.

The model residuals had a normal distribution (Figure 9).

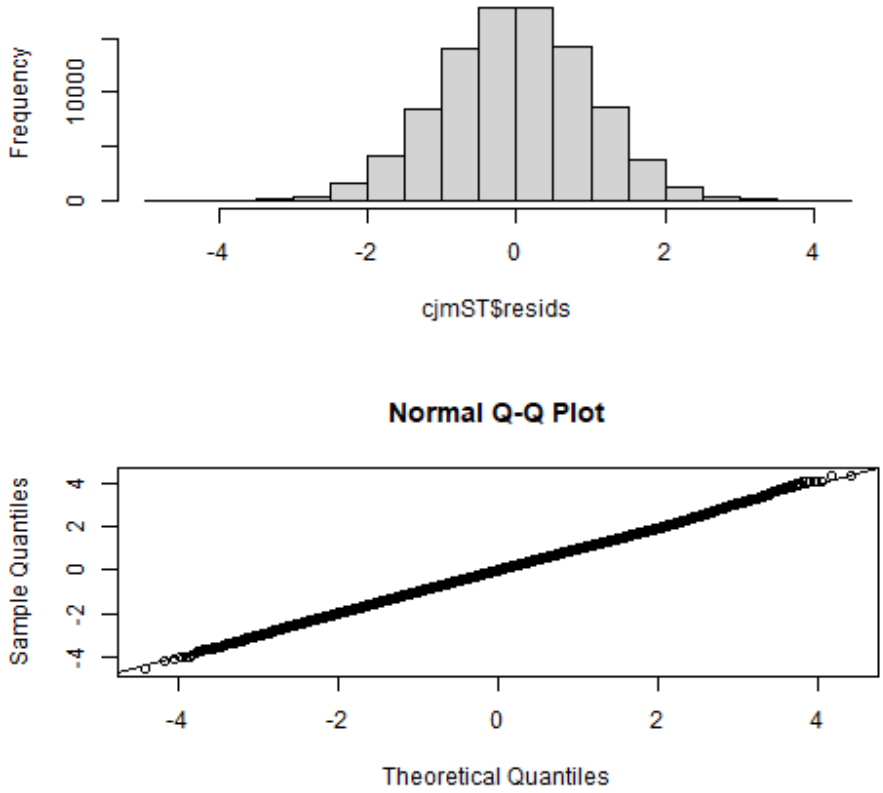

Figure 9. Normal distribution of residuals.

The spatio-temporal random effects are shown in Figure 10, revealing substantial changes over time and space. Higher correlations are observed in the coastal zone during the early years; these then expand longitudinally, and in the most recent years (2023 and 2024) intensify again in the coastal zone.

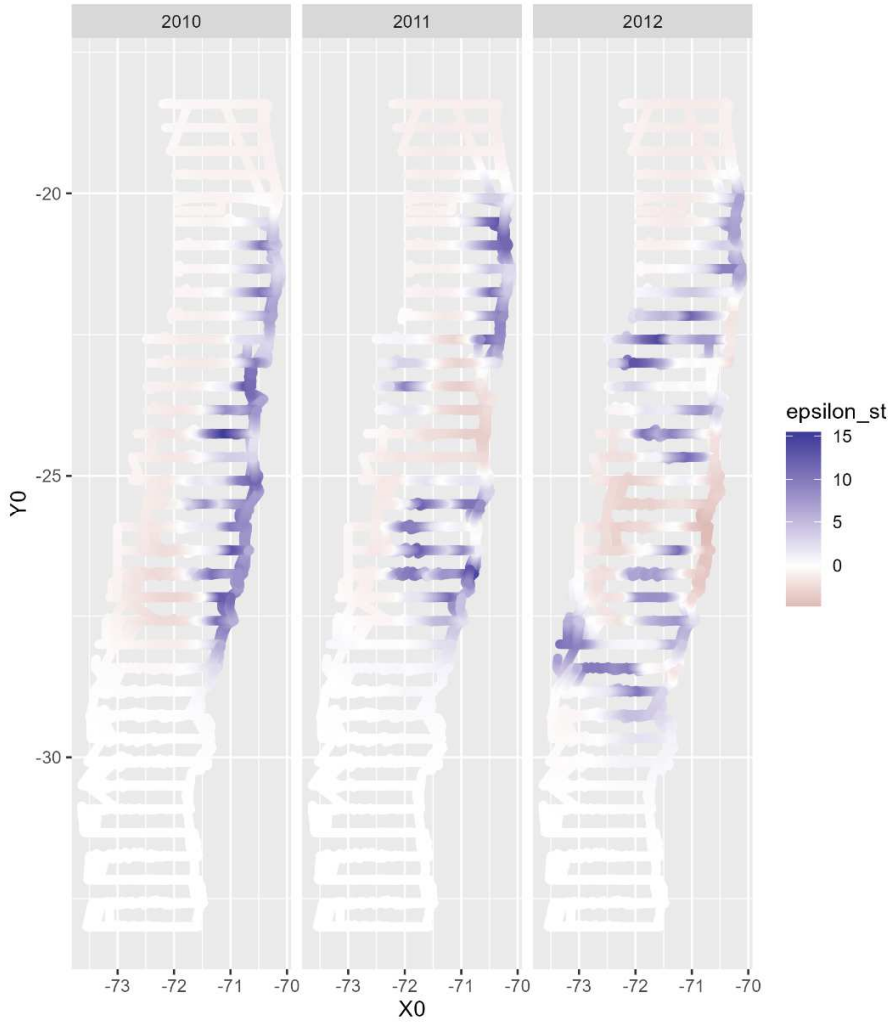

Figure 10. Spatio-temporal random effects by year.

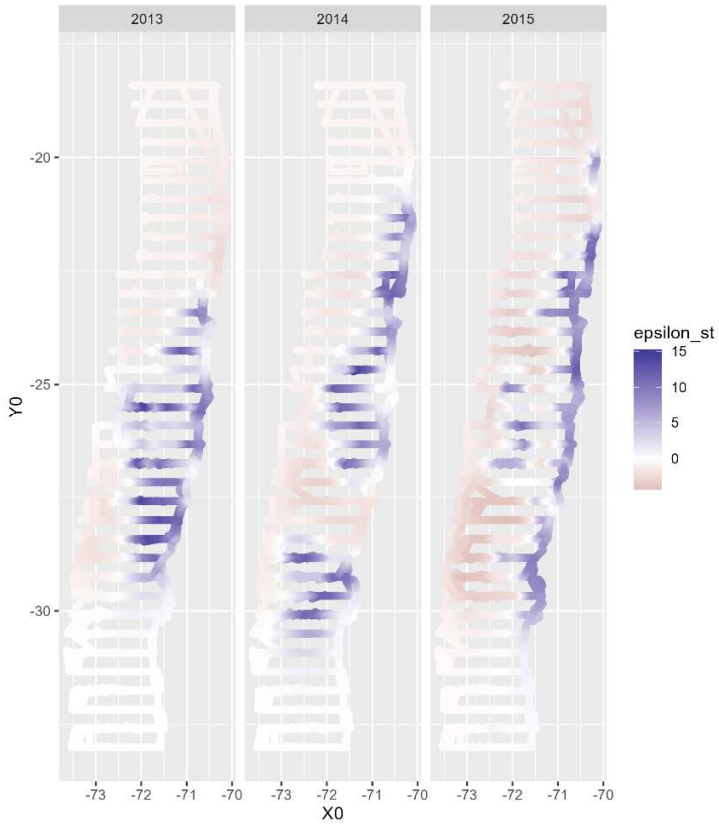

Figure 10. Continuated.

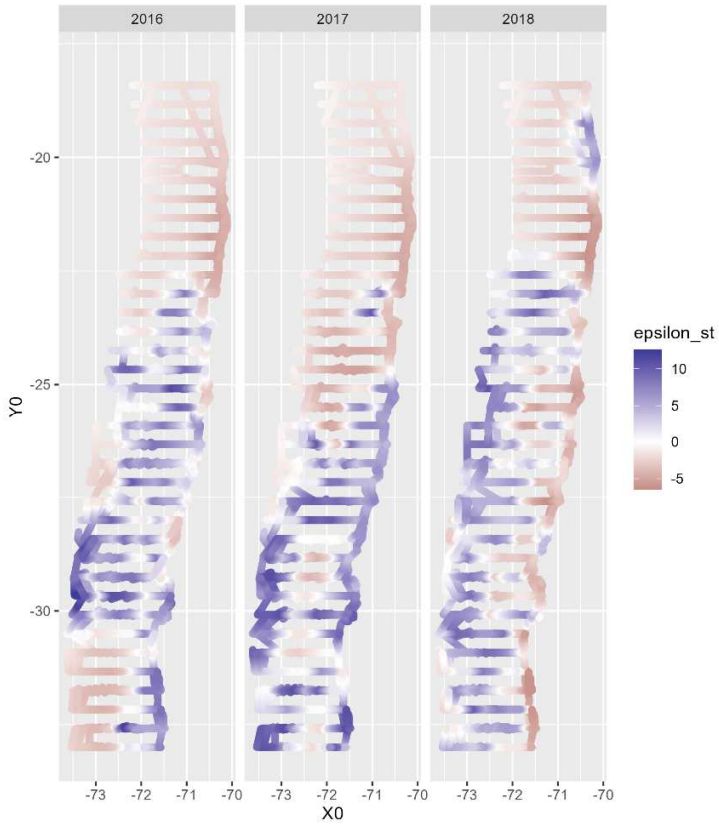

Figure 10. Continuated.

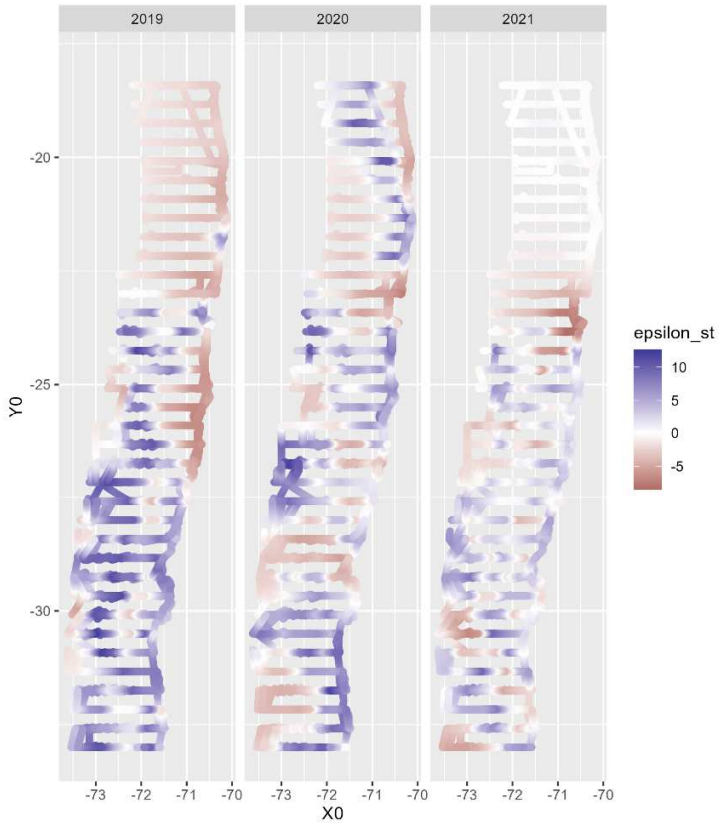

Figure 10. Continuated.

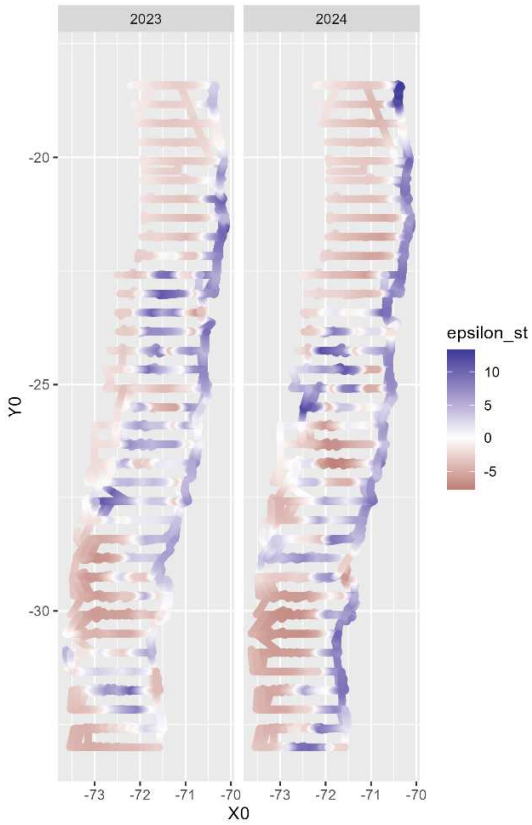

Figure 10. Continuated.

The purely spatial random effects were consistent over time, with higher values observed in the coastal zone and lower values in the northern area (Figure 11).

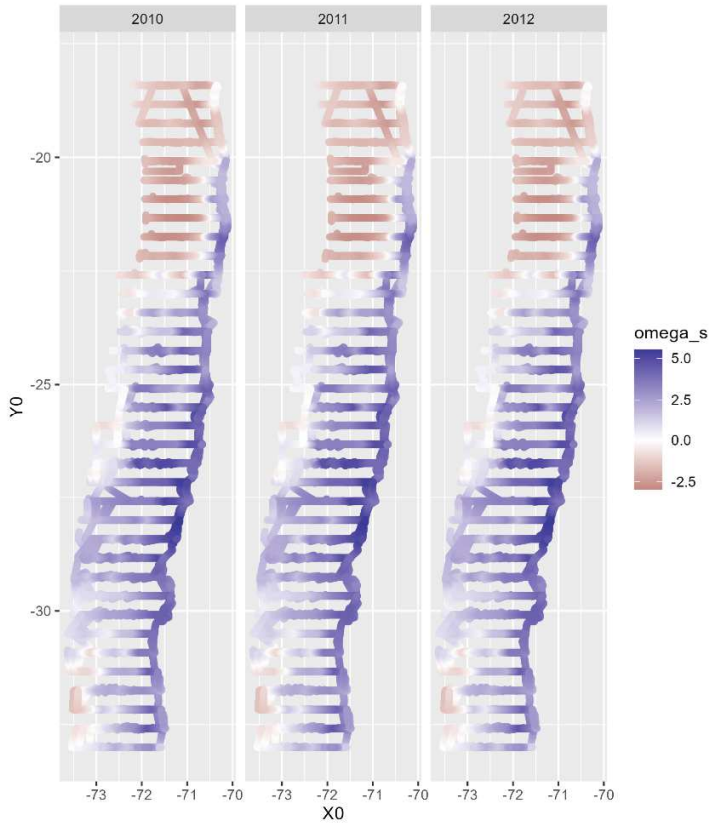

Figure 11. Spatial random effects.

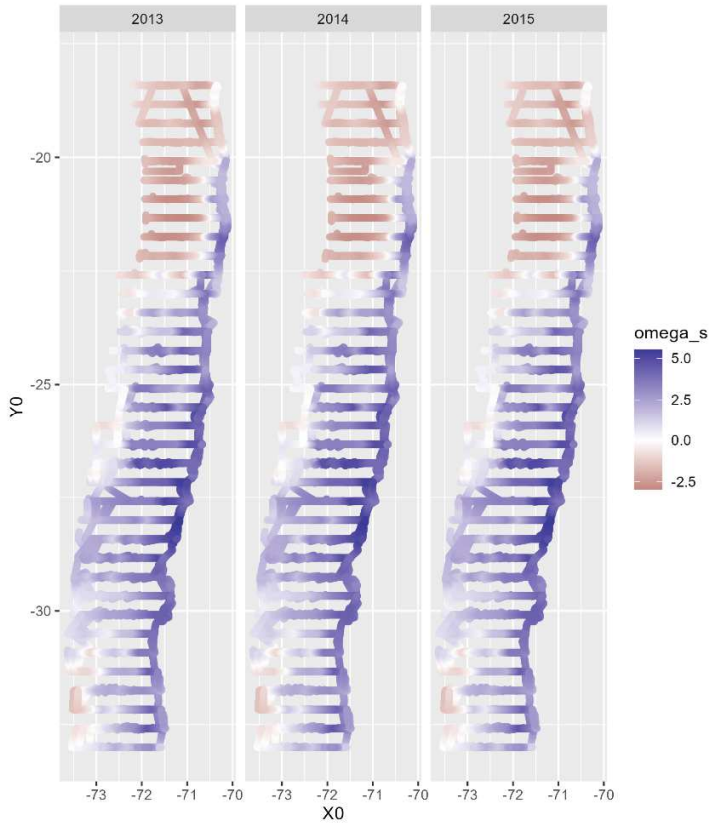

Figure 11. Continuated.

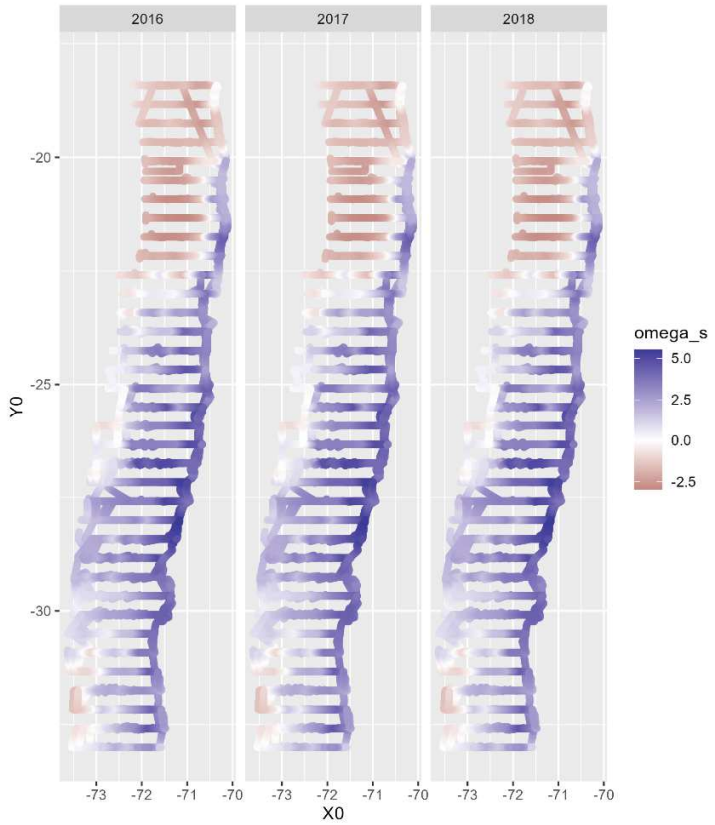

Figure 11. Continuated.

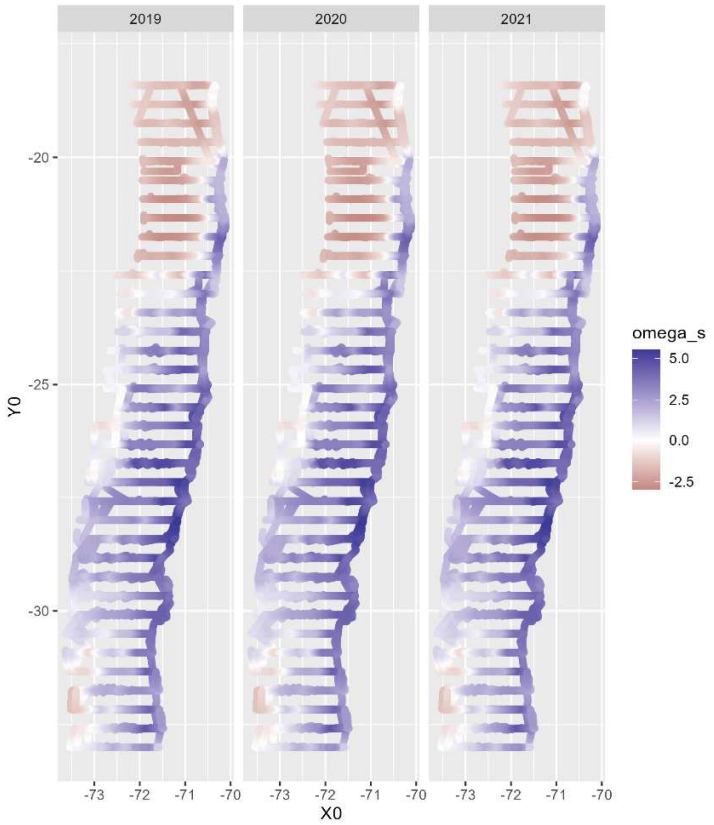

Figure 11. Continuated.

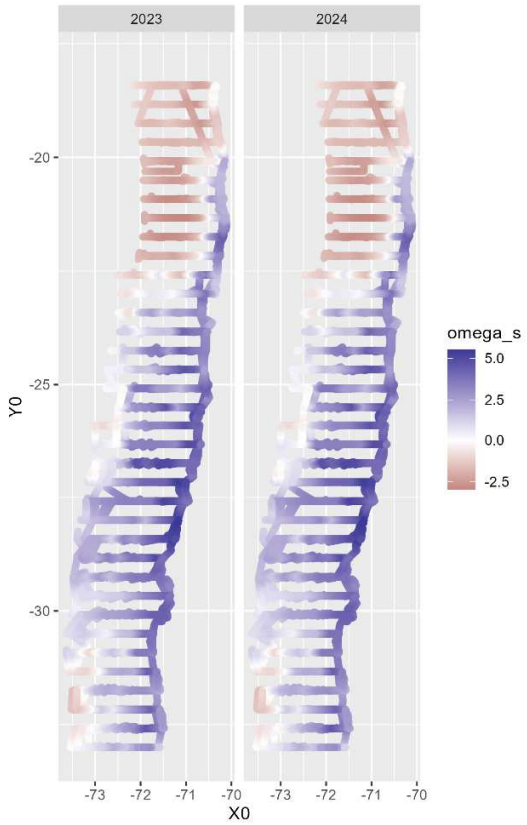

Figure 11. Continuated.

The smoothed effect of oxygen remained stable across the observed oxygen values (Figure 12). Likewise, acoustic density did not exhibit a significant relationship with oxygen (Figure 13).

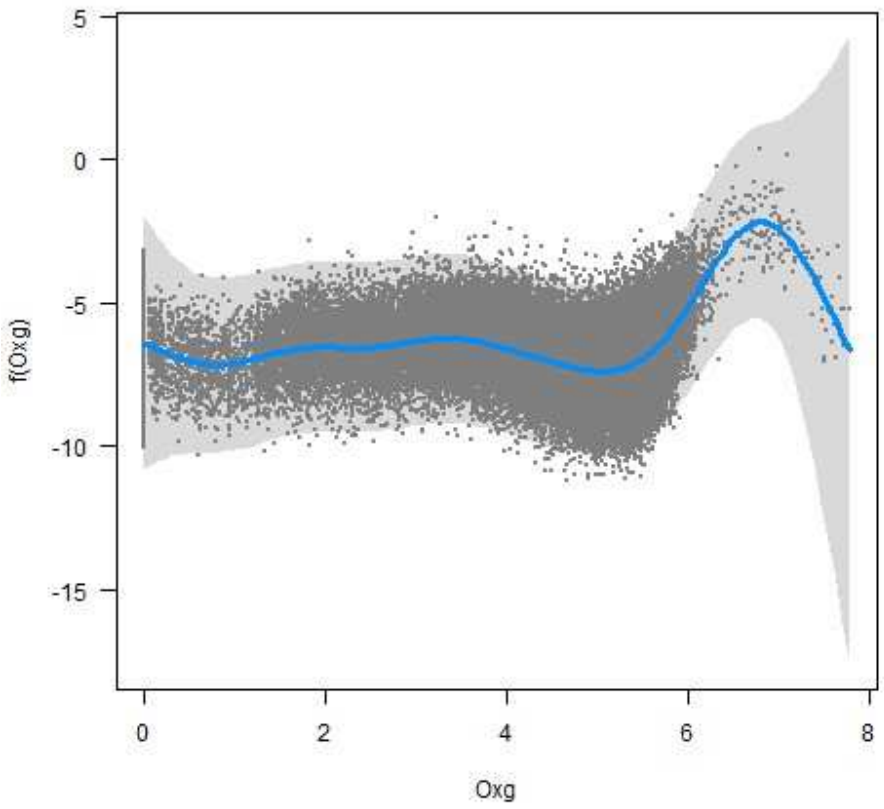

Figure 12. Oxygen transformation function.

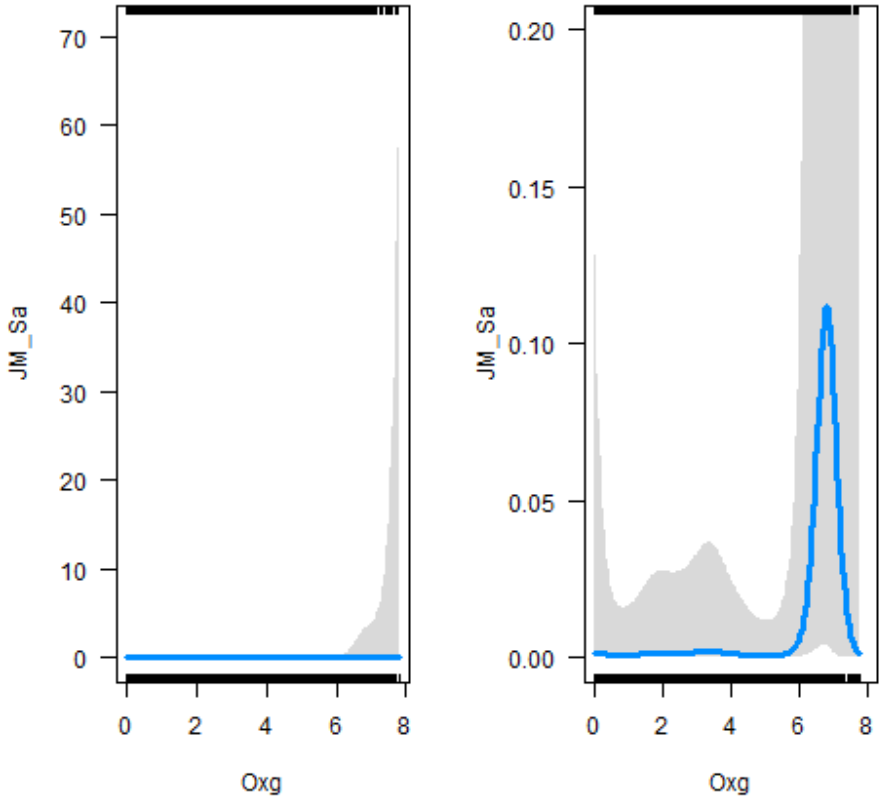

Figura 13. Acoustic density and Oxygen relationship.

The acoustic density index (Sa) remained low from 2010 to 2018 and then increased sharply up to 2024, showing an almost linear trend (Figure 14 and Table 10). The coefficient of variation decreased over time, except in 2011, when the CV was very high (CV = 3.32).

The index for the northern area (<29°S) showed a later increase (starting in 2021) compared to the index for the entire northern zone and reached a lower level of increase in the most recent years (Figure 15 and Table 11).

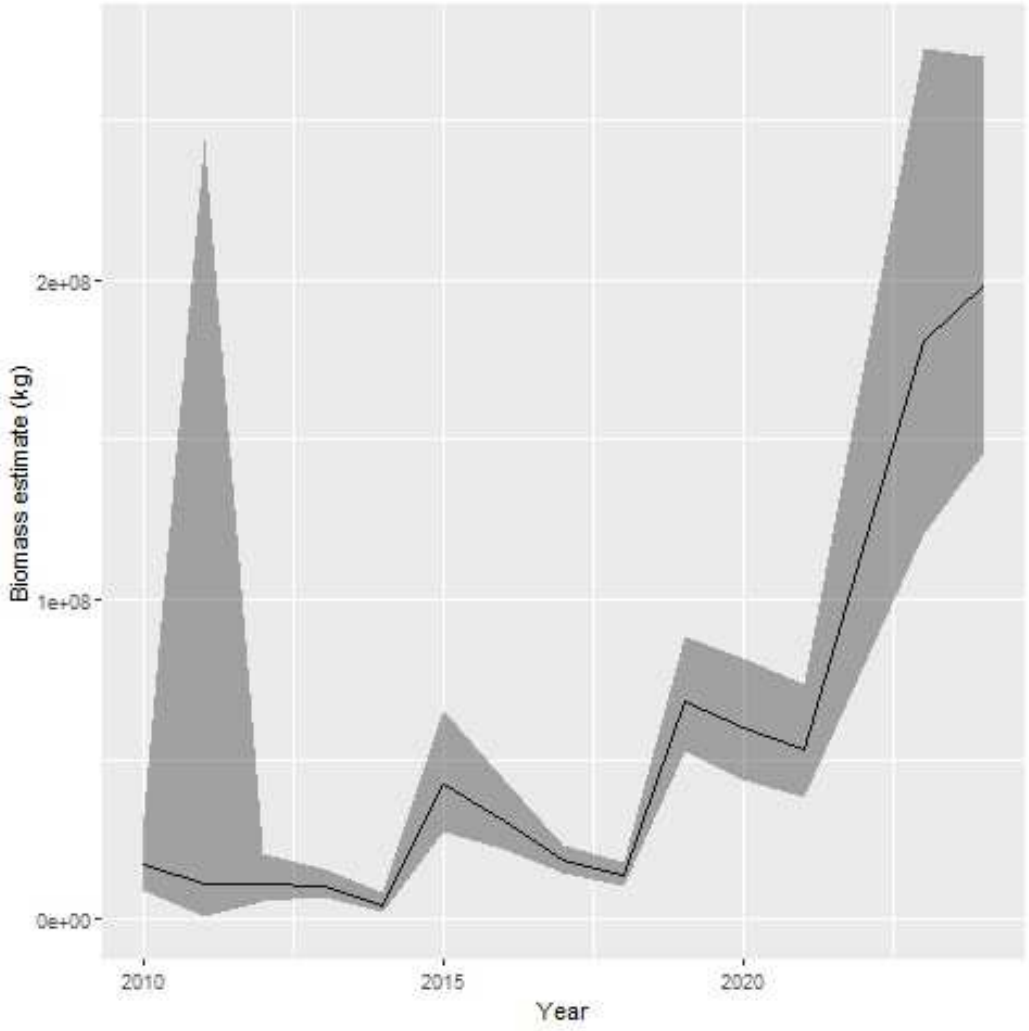

Figure 14. Acoustic density index.

Table 8. Estimates for the northern zone (total area).

	Year	est	lwr	upr	cv
1	2010	16927078	8888160	32236813	0.34
2	2011	11104038	505167	244076828	3.32
3	2012	10802773	5705745	20453054	0.33
4	2013	10170180	6647969	15558521	0.22
5	2014	4113559	1983478	8531159	0.39

6	2015	42034605	26980061	65489403	0.23
7	2016	30607220	21565099	43440649	0.18
8	2017	18239782	14212788	23407770	0.13
9	2018	13314482	10083742	17580322	0.14
10	2019	68015593	52154178	88700870	0.14
11	2020	59599226	43431141	81786196	0.16
12	2021	52913977	38072121	73541712	0.17
14	2023	181021284	120213299	272588021	0.21
15	2024	198537781	146130071	269740857	0.16

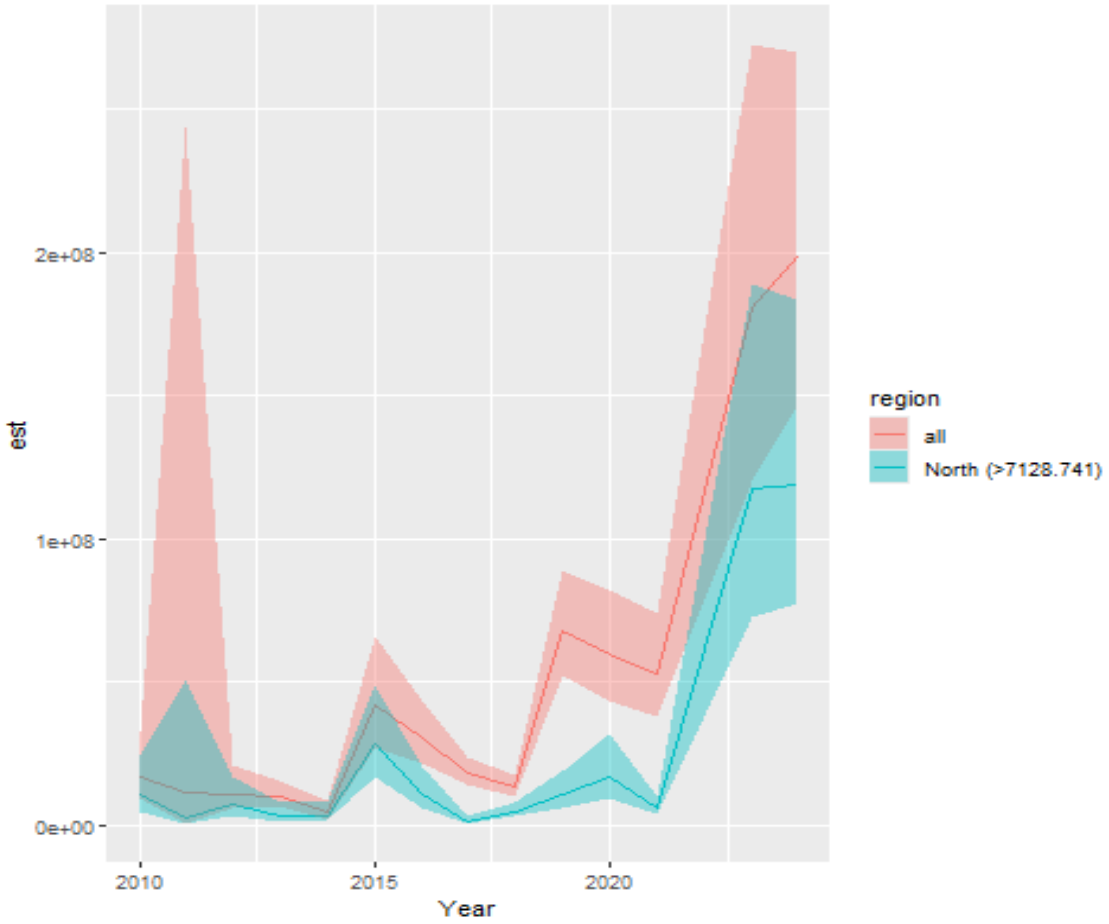

Figure 15. Abundance index for the entire whole zone (“all”) and for the northern area.

Table 9. Estimates for the northern area (fleet 1).

	Year	est	lwr	upr	cv
1	2010	6696421	3248469	13804058	0.38
2	2011	8547245	361750	201949941	3.54
3	2012	3547333	1989992	6323428	0.30
4	2013	6929068	4480074	10716784	0.23
5	2014	698442	348050	1401585	0.37
6	2015	13711021	8674514	21671773	0.24
7	2016	19821186	14294643	27484382	0.17
8	2017	17078165	13292229	21942424	0.13
9	2018	8592885	6465646	11419999	0.15
10	2019	57525677	44190979	74884141	0.14
11	2020	42748037	30904983	59129451	0.17
12	2021	47056702	33346361	66404042	0.18
14	2023	63837972	31045076	131269989	0.38
15	2024	79558844	60251172	105053719	0.14

5. Discussion

The trend of the acoustic density index (Sa) estimated from Model 5 was consistent with the trend of density (t/nm²) estimated annually using the biomass estimation method (Figure 16). This is a notable result, as these series are not fully comparable: acoustic density represents the raw acoustic signal, whereas density expressed in tonnes results from the integration of the acoustic signal with biological information (size-frequency distribution and the length–weight relationship), as well as the length–target strength relationship. Consequently, the observed differences between both indices may be attributed to changes in the population size structure and to variations in the condition factor of the fish.

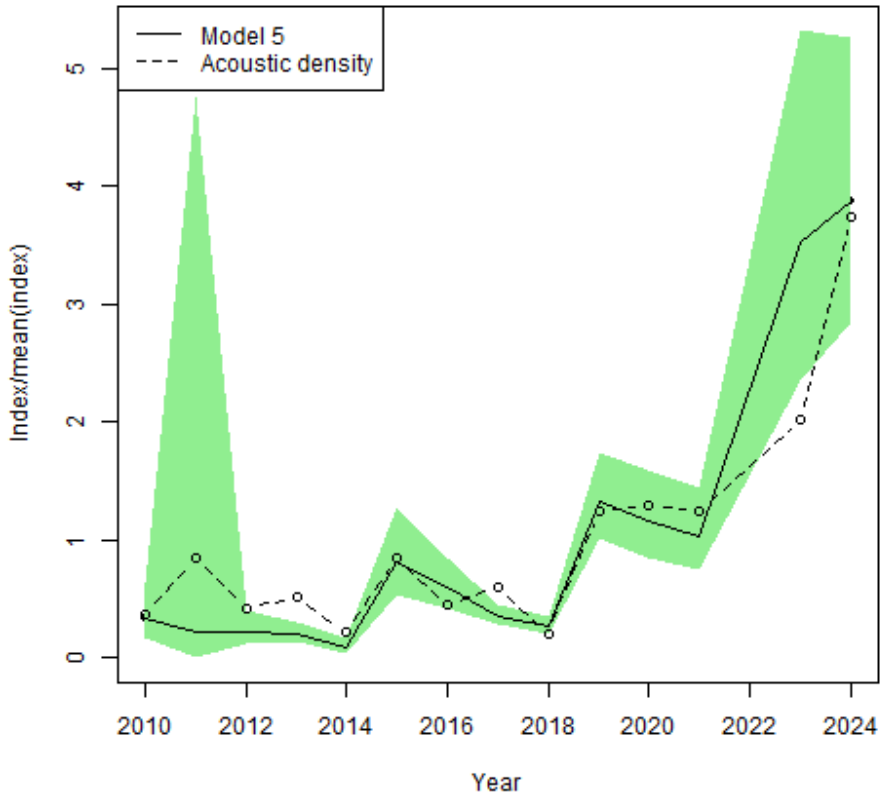

Figure 16. Abundance index from Model 5 and acoustically estimated density.

A similarity was also observed between the trend of the acoustic density index (Sa) estimated from Model 5 and the trend of total biomass estimated annually using the hydroacoustic biomass estimation method (Figure 17). In this case, in order to explain the differences between the series, in addition to the effects of biological information and

target strength, the effect of the area used in the estimation of total biomass must also be considered.

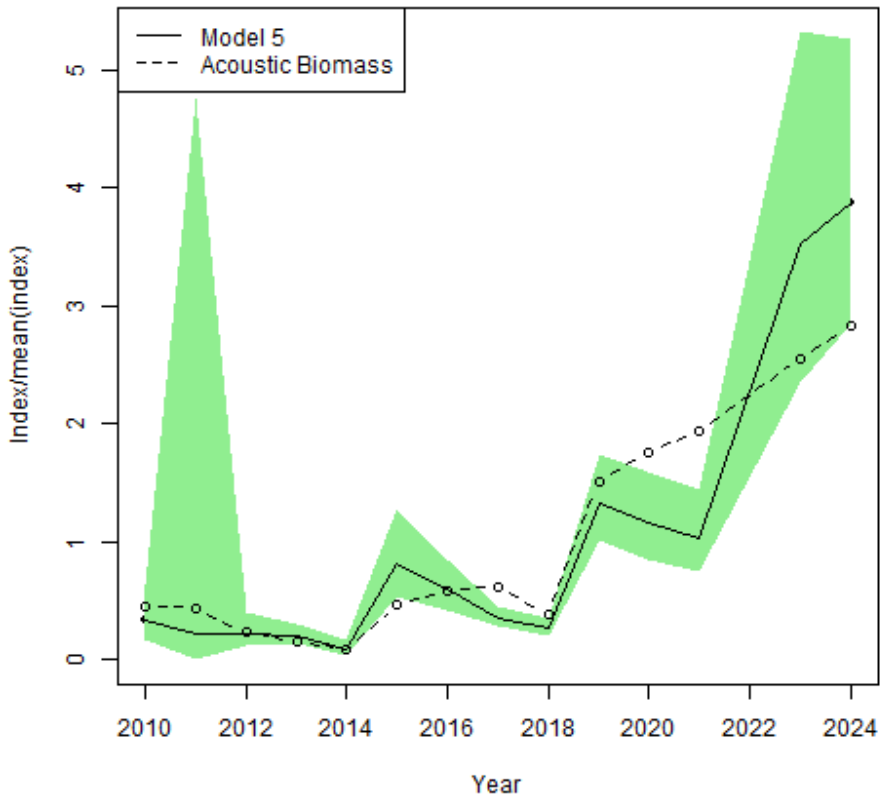

Figure 17. Abundance index from Model 5 and biomass estimated using traditional geostatistical methods.

The Sa index estimated for the northern area (model 5) was also very similar to the density and biomass estimates obtained using hydroacoustic methods (Figures 18 and 19).

The acoustic density index may be particularly informative when the number of trawl hauls is low and when spatiotemporal sampling of length distributions may be biased.

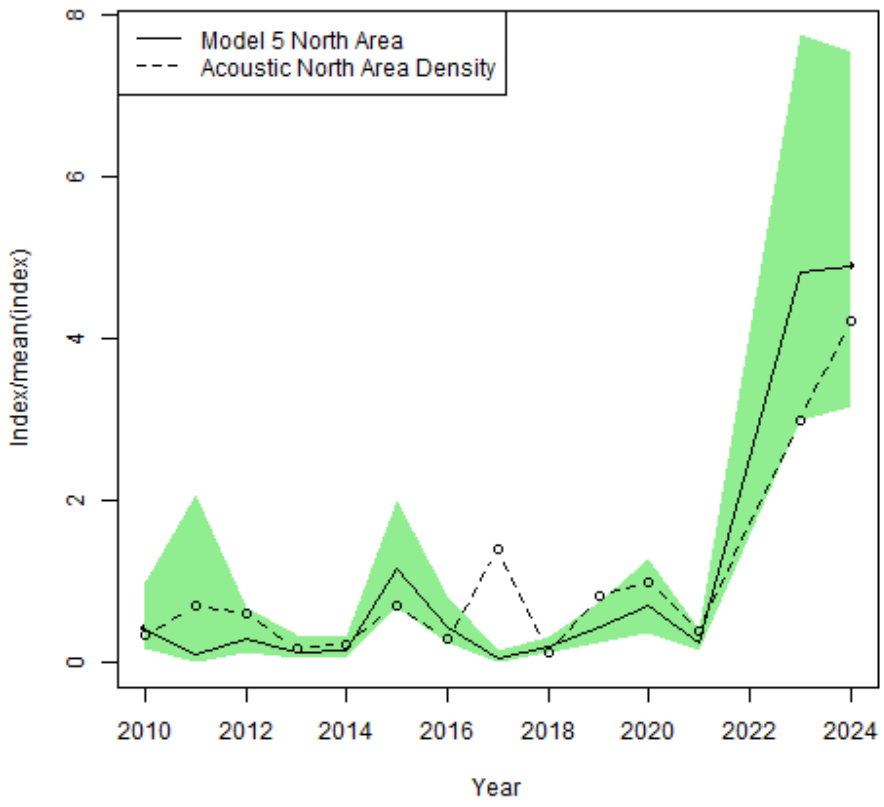

Figure. 18. Abundance index from Model 5 and density estimated using traditional geostatistical methods for the north (fleet 1) area.

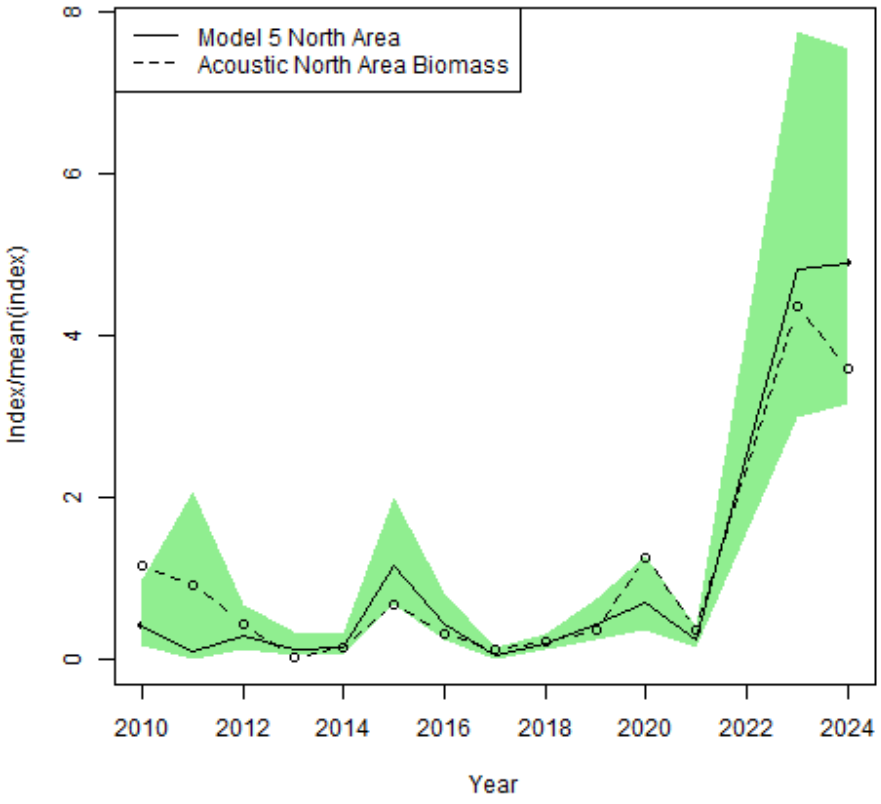

Figure. 18. Abundance index from Model 5 and biomass estimated using traditional geostatistical methods for the north (fleet 1) area.

6. References

Anderson, S.C., E.J. Ward, P.A. English, L.A.K. Barnett. 2022. sdmTMB: an R package for fast, flexible, and user-friendly generalized linear mixed effects models with spatial and spatiotemporal random fields. bioRxiv 2022.03.24.485545; doi: https://doi.org/10.1101/2022.03.24.485545.

Dunn, P. K. (2017). Tweedie: Evaluation of Tweedie exponential family models. R package version 2.3.

McCullagh, P., Nelder, John A. (1989); Generalized Linear Models, Series: Monographs on Statistics & Applied Probability, Chapman & Hall/CRC.